

Phosphorylation of MX2 regulates innate immunity against HIV-1

Gilberto Betancor

King's College London

Jose Jimenez-Guardeño

King's College London <https://orcid.org/0000-0002-1726-8033>

Steven Lynham

King's College London

Robin Antrobus

Cambridge Institute for Medical Research, University of Cambridge

Hataf Khan

University College London

Andrew Sobala

King's College London

Matthew Dicks

King's College London

Michael Malim (✉ michael.malim@kcl.ac.uk)

King's College London <https://orcid.org/0000-0002-7699-2064>

Article

Keywords: HIV-1, innate immunity, interferon, MX2, nuclear import, myosin light chain phosphatase, MYPT1, PPP1CB, regulatory phosphorylation

Posted Date: March 29th, 2021

DOI: <https://doi.org/10.21203/rs.3.rs-274544/v1>

License: (cc) (i) This work is licensed under a Creative Commons Attribution 4.0 International License.

[Read Full License](#)

Phosphorylation of MX2 regulates innate immunity against HIV-1

Gilberto Betancor^{1*}, Jose M Jimenez-Guardeño¹, Steven Lynham², Robin Antrobus³, Hataf Khan¹, Andrew E Sobala¹, Matthew DJ Dicks¹ & Michael H Malim^{1*}

¹Department of Infectious Diseases, School of Immunology & Microbial Sciences, King's College London, London SE1 9RT, UK

²Centre of Excellence for Mass Spectrometry, The James Black Centre, King's College London, London SE5 9NU, UK

³Cambridge Institute for Medical Research, Department of Medicine, University of Cambridge, Cambridge CB2 0XY, UK

*Co-corresponding authors

Department of Infectious Diseases, School of Immunology & Microbial Sciences, King's College London, 2nd Floor Borough Wing, Guy's Hospital, London Bridge, London, SE1 9RT
tel: +44 20 7848 9606

email: michael.malim@kcl.ac.uk, gilberto.betancor@kcl.ac.uk

Summary

Interferon (IFN) mobilizes a cellular anti-viral state by inducing the expression of IFN-stimulated genes (ISGs). Myxovirus resistance 2 (MX2/MxB) is an ISG that inhibits HIV-1 infection by suppressing viral import into the nucleus. The amino-terminal domain (NTD) of MX2 plays an essential role in viral inhibition and, here, we exploit proteomic screening to identify the myosin light chain phosphatase (MLCP) components MYPT1 and PPP1CB as key NTD binding partners. Experimental depletion of either protein, or pharmacologic inhibition of MLCP, reduces MX2 anti-viral activity. Analysis of post-translational modifications defined sites of phosphorylation within the NTD, and replacement of the serines at positions 14, 17 and 18 with the phosphomimetic aspartic acid phenocopies MLCP silencing by abrogating anti-viral function. Phosphorylation of this triple-serine motif impedes MX2's interaction with its HIV-1 protein target, Capsid, reduces MX2 accumulation at the nuclear envelope, and weakens MX2's ability to inhibit the nuclear import of non-viral karyophilic cargo. Finally, IFN itself acts to reduce levels of phosphorylation at these key regulatory serines. We therefore propose that homeostatic repression of MX2 through NTD phosphorylation, together with its reversal by MLCP and IFN, balances the deleterious effects of MX2 on normal cell function with innate immunity against HIV-1.

Keywords: HIV-1, innate immunity, interferon, MX2, nuclear import, myosin light chain phosphatase, MYPT1, PPP1CB, regulatory phosphorylation

Introduction

Type 1 interferons (IFNs) are produced following recognition of pathogen-associated markers by cell-encoded pattern recognition receptors. In response to IFN, a cascade of genes known as IFN stimulated genes (ISGs) are induced, establishing an anti-viral state within the infected host^{1,2}. Myxovirus resistance 2 (MX2/MxB) is an ISG with potent inhibitory activity against HIV-1 as well as herpesviruses and hepatitis B virus (HBV)³⁻¹⁰. MX2 inhibits HIV-1 infection prior to the nuclear import of viral pre-integration complexes, but after reverse transcription^{3,4,11}. Pivotal to HIV-1 inhibition is recognition of the viral capsid, since point mutations in the Capsid (CA) protein can render the virus insensitive to MX2^{3-5,12,13}.

MX2 belongs to the dynamin-like family of GTPases and is closely related to MX1 (MxA), another ISG which has broad inhibitory activity for a variety of RNA and DNA viruses, including influenza A virus (IAV) and HBV¹⁴⁻¹⁶. Unlike MX1, where a conserved loop in the stalk domain (loop 4) is critical for restriction of IAV¹⁷⁻²⁰, the amino-terminal domain (NTD) is the principal determinant of MX2's activity against HIV-1^{21,23}. For instance, transfer of this domain to proteins devoid of HIV-1 inhibitory activity confers robust anti-viral activity²¹⁻²⁵.

The NTD also determines the localization of MX2 to the nuclear envelope^{25,26}. Three conserved arginine residues at positions 11 to 13 in the NTD have been shown to be required for anti-viral activity^{25,26}, to be important for CA binding²⁷⁻²⁹, and to be involved in interactions with nuclear pore proteins such as NUP214 and the nuclear transport receptor transportin 1 (TNPO1)²⁵. In light of the NTD's fundamental role in MX2 function, we used stable isotope labelling by amino acids (SILAC) and a panel of engineered MX constructs to identify additional cellular factors that interact with MX2. By focusing on the critical arginine motif, we discovered that the myosin light chain phosphatase (MLCP) subunits MYPT1 and PPP1CB interact with the NTD. Pharmacologic inhibition or targeted depletion of MLCP impeded the ability of MX2 to inhibit HIV-1. We further found that MX2 is phosphorylated at different

positions in the NTD, and that serine phosphorylation at positions 14, 17 and 18 blocks anti-viral activity, affects localization to the nuclear envelope, and prevents the interaction with HIV-1 CA. Finally, we present evidence that phosphorylation of these serines also suppresses the capacity of MX2 to interfere with the nuclear import of cellular karyophilic cargo, therefore providing cells with a mechanism for averting the deleterious effects of disrupted nuclear trafficking in the absence of virus infection.

Results:

The N-terminal domain of MX2 interacts with MYPT1 and PPP1CB

To understand in greater detail the mechanistic basis for MX2 function, we used the retrieval of tagged proteins from transfected 293T cells to identify interacting cellular proteins. Specifically, we performed SILAC-based screens with a series of MX protein and control constructs that enabled four pairwise comparisons: MX2 versus MX1, MX2 versus mock transfection, MX2 versus a non-functional mutant where the arginines at positions 11 to 13 had been replaced with alanine (R11-13A)²³, and green fluorescent protein (GFP) versus a GFP (NTD_{MX2}) chimaera. Two interacting proteins were consistently enriched in samples obtained using proteins bearing the wild type MX2 NTD (i.e., MX2 and GFP (NTD_{MX2})): myosin phosphatase target subunit 1 (MYPT1) and protein phosphatase 1 catalytic subunit beta (PPP1CB) (Fig. 1a). As expected, owing to its ability to oligomerize^{24,30}, MX2 itself was also enriched in all comparisons except MX2 vs MX2 R11-13A.

MYPT1 and PPP1CB, together with the small subunit M20, assemble to form a holoenzyme known as myosin light chain phosphatase (MLCP), a member of the serine/threonine protein phosphatase 1 (PP1) family³¹. For this holoenzyme, PPP1CB is the catalytic subunit (PP1c), while MYPT1 serves as a regulatory factor. PP1 complexes are able to interact with their substrates through a variety of motifs³². One of these, comprising the sequence F-X-X-R-X-R, has been found in the cytosolic RNA sensors MDA5 and RIG-I, and acts as a binding site for other PP1 catalytic subunits (PPP1CA and PPP1CC)³³. Notably, a variant of this motif (⁸W-P-Y-R-R-R¹³) is present in the MX2 NTD (Fig. 1b) and harbours the three arginines at positions 11, 12 and 13, explaining why MYPT1 and PPP1CB were enriched for binding to wild type MX2 relative to MX2 R11-13A (Fig. 1a). Additional confirmation of this interaction was obtained in co-immunoprecipitation experiments where MX2 and GFP

(NTD_{MX2}), but not MX1, MX2 R11-13A or GFP (NTD_{MX2}) R11-13A were able to pull-down endogenous PPP1CB and MYPT1(Fig. 1c).

MLCP regulates the anti-viral activity of MX2

We next addressed the impact of MLCP on the anti-viral activity of MX2. U87-MG CD4⁺ CXCR4⁺ cells, a well-established *in vitro* model for studying HIV-1 replication^{3, 9, 21, 23-25, 28}, expressing MX2 or the control protein luciferase (Luc) were transfected with pools of four siRNAs directed against PPP1CB or MYPT1, or a control (CTR) siRNA. In cells treated with CTR siRNA, infection with an HIV-1 based lentiviral vector (HIV-1/GFP) was ~10-fold lower in cells expressing MX2 (Fig. 2a), consistent with previous data^{21,23-25}. In cells depleted of PPP1CB or MYPT1 the suppressive effect of MX2 was reduced to ~5-fold; the partial nature of these effects is likely attributable to incomplete silencing (Fig. 2b). Analysis of individual constituent siRNAs yielded variable results with one MYPT1 and two PPP1CB siRNAs recapitulating the phenotypes of the pools (Supplementary Fig. 1a). Critically, increases in infection were not observed following MYPT1 or PPP1CB silencing in the presence of MX2 when cells were challenged with MX2-insensitive viruses based on murine leukemia virus (MLV) or bearing the MX2-resistant HIV-1 CA mutation P90A (Fig. 2a). Additionally, cells doubly depleted of PPP1CB and MYPT1 did not display a further loss of MX2 anti-viral activity, relative to individual knock-downs, suggestive of their activities being mediated through a common pathway (Supplementary Fig. 1b). Finally, ectopic expression of MYPT1, but not PPP1CB, in MX2 expressing U87-MG CD4⁺ CXCR4⁺ cells reduced the inhibitory effect of MX2 (Supplementary Fig. 2a), an effect likely due to the ability of ectopically expressed MYPT1 to impair the interaction of MX2 with endogenous PPP1CB (Supplementary Fig. 2b). Such dominant-negative behaviour further links MYPT1/MLCP function to the anti-viral activity of MX2.

There are a number of pharmacologic inhibitors of protein phosphatases. Okadaic acid inhibits both PP1 and PP2 (the other main serine/threonine protein phosphatase) but is far more potent against the latter (IC₅₀ values ranging from 60 to 500 nM, versus 1 nM, respectively). Calyculin A has a similar activity profile for both (IC₅₀ of 0.5-1 nM) and therefore inhibits PP1 at lower concentrations than okadaic acid. Finally, rubratoxin A is a PP2 specific inhibitor³⁴⁻³⁸. Concentrations of calyculin A as low as 2.25 nM yielded significant reductions in MX2 activity (Fig. 2c), whereas much higher concentrations of okadaic acid (from 30 nM) were required to produce a similar effect and even the highest tested concentration of rubratoxin A (50 µM) had no effect. Finally, the specificity of these drug effects was confirmed in MLV challenges of U87-MG CD4⁺ CXCR4⁺ cells where any viral suppression was equivalent in Luc or MX2 expressing cells at all concentrations tested (Supplementary Fig. 2c). Altogether, these data implicate MLCP, a PP1, as a novel regulator of MX2-mediated HIV-1 inhibition.

Lack of functional MLCP disrupts MX2's ability to inhibit viral infection during the IFN response

We then asked whether endogenous MX2 (expressed following IFN exposure) is regulated by MLCP. We used bulk and clonal cell populations (two) derived from U87-MG CD4⁺ CXCR4⁺ cells where the endogenous *MX2* alleles had been inactivated using CRISPR-Cas9 genome editing, as well as a control line (CTR CRISPR)²⁵. Cells were transfected with siRNAs specific for MX2 (positive control), MYPT1, or PPP1CB, or a CTR siRNA, before being incubated for 24 h in the presence or absence of IFN. As previously established, IFN-mediated viral suppression was severely impaired in all three MX2 knock-out cultures compared to CTR CRISPR cells (~3-fold reduction in infection compared to ~12-fold, respectively) (Fig. 3a). Critically, significant losses in the anti-viral activity of IFN were apparent when MYPT1 or PPP1CB were depleted in CTR cells, but this ameliorating effect was dependent on MX2-mediated suppression and was not therefore seen in any of the *MX2*-knock-out lines (Fig. 3b

shows corresponding analyses of protein levels). Complementing these data, calyculin A also partially reversed the effect of IFN, but again this was limited to CTR cells and not cells lacking MX2. (Fig. 3a). Of note, and consistent with earlier findings (Fig. 2a), the modest inhibition of MLV infection by IFN was unaffected by the absence of MX2 or by the depletion of MYPT1 or PPP1CB, again associating MX2 function with MLCP activity (Supplementary Fig. 3).

We next addressed whether MYPT1 and PPP1CB contribute to the IFN-induced suppression of HIV-1 in primary human CD4⁺ T cells, the principal target of viral infection *in vivo*. Short hairpin RNAs (shRNAs) specific for MX2, MYPT1 or PPP1CB as well as a negative control (scrambled sequence) were delivered by lentiviral vector transduction. In all four donors, depletion of any of these genes resulted in reduced inhibition of HIV-1 by IFN (Fig. 3c; Fig. 3d shows the mRNA levels). Similarly, inhibition of PP1 using calyculin A reduced the anti-viral effect of IFN in all seven donors analyzed (Fig. 3e). These findings confirm the role of MLCP in the IFN-mediated inhibition of HIV-1 and demonstrate that their activity is channeled through MX2.

MX2 anti-viral activity is regulated by serine phosphorylation

Based on the aforementioned data, we predicted that MLCP dephosphorylates functionally important residues in the MX2 NTD. We therefore used LC-MS/MS to identify post-translational modifications in MX2 expressed in 293T cells. By focusing on the NTD, we identified modified peptides that revealed that MX2 is phosphorylated at the serines at positions 14, 17, 18, 28 and 78, and the threonines at 38 and 67 (Fig. 4a; Supplementary Fig. 4a). While 99% of MX2's sequence was covered by multiple peptides, peptides corresponding to the amino-terminal 20 amino acids were underrepresented. Critically, of the 42 peptides identified within this N-terminal region, 19 were phosphorylated at positions 14, 17 or 18. Owing to the close proximity of these modified residues, often lying within a single LysC

digested peptide, estimates of relative peptide abundances were therefore calculated using chromatographic peak areas (Supplementary Fig. 4b): it is apparent that all three serines are frequently phosphorylated when comparing areas from unmodified peptide with phosphorylated ones, especially S14.

We next explored the biological impact of these findings by replacing the seven serine/threonine residues (individually or in combination for S14, S17 and S18) with alanine to block phosphorylation, or with the phosphomimetic aspartic acid (Fig. 4b). All mutations of S28, T38, T67 or S78 maintained strong HIV-1 inhibitory activity indicating that phosphorylation at these positions does not diminish function (Fig. 4b). In contrast, the triple S14, 17-18D mutation (which we suggest equates to a MLCP-null scenario) rendered MX2 inactive whereas the triple-alanine substitution was as active as the wild type protein. Further corroboration of this phenotype was obtained with the chimeric proteins MX1 (NTD_{MX2}) or Fv1b (NTD_{MX2}), which were also inactive when bearing the S14, 17-18D substitutions (Supplementary Fig. 5a). Individual substitutions of S14, S17 or S18 with aspartic acid yielded proteins with intermediate anti-viral phenotypes, while double substitutions of residues 14 and 17 or 14 and 18, but not as evidently 17 and 18, produced proteins with virtually no anti-viral activity (Supplementary Fig. 5b).

Owing to the functional importance of phosphorylation at these three serines, we generated a polyclonal antiserum using a peptide antigen containing S14, S17 and S18 in their phosphorylated form. This antiserum (anti-P-NTD) detects wild type MX2 and all proteins with at least one aspartic acid substitution, but not the version with the triple S14, 17-18A substitution (Fig. 4c). Importantly, we were able to use this antiserum to confirm that depletion of PPP1CB with siRNA (Fig. 4d), or inactivation by treatment with calyculin A (Fig. 4e), directly increased the level of phosphorylation of the S14-S17-S18 motif (~3-fold and ~5-fold, respectively). As controls, detection of the MX2 S14, 17-18D was noted as being unaffected by altering MLCP activity.

To link further MLCP function with MX2 anti-viral activity, we depleted PPP1CB from U87-MG CD4⁺ CXCR4⁺ cells expressing wild type MX2 or the S14, 17-18A derivative and determined the ability of these proteins to inhibit HIV-1 infection relative to cells receiving control siRNA. Consistent with our previous data, PPP1CB depletion only reduced the anti-viral activity of MX2, while the S14, 17-18A mutant was unaffected (Fig. 4f). These results therefore confirm the role of MLCP as a key regulator of the phosphorylation status and anti-viral activity of MX2.

Phosphorylation of serines 14, 17 and 18 prevents the interaction of the MX2 N-terminal domain with HIV-1 Capsid

Having revealed the importance of phosphorylation at positions 14, 17 and 18 for neutralizing MX2 anti-viral activity, it was important to assess effects on ligand interactions. We and others have previously shown that MX2 specifically interacts with CA and capsid-nucleocapsid (CANC) assemblies *in vitro*^{22,28,29,39}; we therefore used CANC complexes and whole cell lysates from transfected 293T cells expressing MX1 (negative control), wild type MX2 or the S14, 17-18D mutant to examine CA binding. As seen in the pellet samples, phosphorylation at these positions severely inhibited binding to CA (Fig. 5a), however, presumably due to the second CA-interacting domain in the G domain of MX2²⁸, binding was not fully abolished. Introduction of these substitutions into GFP (NTD_{MX2}) demonstrated that phosphorylation at these serines completely prevents the NTD's interaction with HIV-1 CA (Fig. 5a), an attribute that is necessary for MX2 anti-viral function^{27,28}. As additional confirmation of the requirement for an unphosphorylated NTD for interacting with CA, GFP (NTD_{MX2}) expressed in control cell lysates interacted with CANC assemblies, but failed to do so when expressed in cells depleted of PPP1CB (Fig. 5b).

Serine phosphorylation modulates MX2 nuclear envelope localization and the import of karyophilic cargo

MX2 localizes to the nuclear envelope and nuclear pore complexes due to the presence of a targeting signal located within the amino-terminal 25 amino acids^{4,27,40}, and this has been proposed to be important for the suppression of HIV-1 nuclear import^{4,25}. We therefore asked whether phosphorylation of serines 14, 17 and 18 affected the sub-cellular localization of MX2. Indeed, using U87-MG CD4⁺ CXCR4⁺ or HeLa cells stably expressing MX2, we found that S14, 17-18D triple mutation significantly reduced MX2 accumulation at the nuclear envelope, as quantified here as percentage of protein colocalizing (Manders' coefficient) with the nuclear pore complex component NUP358/RanBP2 (Fig. 5c).

It has been recently shown that MX2 interferes with the functionality of different non-viral nuclear localization signals (NLS)²⁶. To test the importance of phosphorylation at residues 14, 17 and 18 for this activity, we used a set of ten different GFP-LacZ chimeric proteins tagged at the amino-terminus with different NLSs and observed their nuclear accumulation in HeLa cells expressing MX1, MX2 or the S14, 17-18D mutant. While we could not discern clear differences with most NLS substrates (Supplementary Fig. 6), this was not the case for hnRNP K (KNS)-GFP-LacZ where significantly more pronounced nuclear localization was evident in cells expressing the S14, 17-18D mutant compared to the wild type, indicating that phosphorylation at these positions impedes MX2's ability to suppress the nuclear transport of cellular cargo (Fig. 6a, b). Additionally, we also noted that introduction of the S14, 17-18D mutation into NTD_{MX2}-GFP-LacZ abolished its nucleoplasmic targeting (Supplementary Fig. 6), reinforcing the notion that phosphorylation of these serines modulates MX2 NTD function at the nuclear envelope/ nuclear pore.

We recently reported that MX2 interacts with the nuclear pore protein NUP214 and the import receptor TNPO1, and that these interactions are important for MX2 anti-viral activity²⁵. We therefore evaluated the interaction of MX2 S14, 17-18D with both proteins by co-immunoprecipitation, and found that the presence of non-phosphorylated residues at these positions is essential for binding to both NUP214 and TNPO1 (Fig. 6c).

IFN modulates MX2 NTD phosphorylation

In a final experiment, we sought additional insight into the regulation of phosphorylation at the S14-S17-S18 motif by assessing the influence of IFN. U87-MG CD4⁺ CXCR4⁺ cells expressing Flag-tagged MX2 were treated with IFN for 24 h, and the level of phosphorylated MX2 analyzed by immunoblot using anti-P-NTD and anti-Flag antibodies. Strikingly, phosphorylation at the triple-serine motif was significantly reduced in the presence of IFN (Fig. 6d); a similar result was also obtained when analysing a chimeric RFP (NTD_{MX2}) protein (Fig. 6e). Based on our data showing that dephosphorylation of these serines is required for MX2 anti-viral function, we therefore propose that IFN induces MX2 function through a combination of post-translational and transcriptional mechanisms.

Discussion

MX2 is one of the major post-entry restriction factors for HIV-1, accumulating at the nuclear envelope and inhibiting viral entry into the nucleus. The NTD plays a pivotal role in MX2 function, and contains the R11-13 motif which is essential for viral inhibition and the interaction with the viral capsid^{11,21-23, 27-29,39}. Here, we report SILAC-based interaction screens that identified MYPT1 and PPP1CB as novel MX2 interacting proteins (Fig. 1). Both proteins are components of MLCP, a member of the PP1 family of cellular phosphatases. PP1 complexes engage a variety of substrates through multiple binding motifs (reviewed in ref⁴¹) and are involved in myriad biological processes including muscle contraction, cell division and the regulation of virus replication^{31,38,42,43}. The W-P-Y-R-R-R sequence (residues 8 to 13) found in the MX2 NTD represents a good match with one PP1 consensus binding site, and co-immunoprecipitation confirmed that MYTP1 and PPP1CB interact with this sequence (Fig. 1c).

Gene silencing experiments demonstrated that depletion of MYPT1 or PPP1CB reduces the anti-viral potency of MX2 (Fig. 2a), whereas simultaneous knock-down failed to reduce further anti-viral activity supporting our conclusion that MYPT1 or PPP1CB act through a common factor or pathway, namely MLCP. The role of MLCP in regulating MX2 function was further validated in experiments using established pharmacological inhibitors of protein phosphatases (Fig. 2c). Importantly, parallel analyses using either the MX2-insensitive virus MLV or the HIV-1 CA mutant P90A failed to show any effects on infectivity, demonstrating the selectivity of MLCP action in promoting MX2-mediated inhibition of wild type HIV-1 infection. Because MX2 is an ISG, it was also important to verify the role of MLCP during the IFN-mediated anti-viral response. Accordingly, we depleted endogenous MX2 to show that the reductions in the inhibitory effects of IFN that are observed following MLCP silencing or inhibition are reliant on MX2 (Fig. 3a), and confirmed that MLCP is required for the full IFN-induced suppression of HIV-1 in primary CD4⁺ T cells (Fig. 3c, e).

We turned to mass spectrometry to define the post-translational modifications of MX2 (Fig. 4). Focusing on the NTD, we discovered that serine phosphorylation at positions 14, 17 and 18 regulates anti-viral function: when unphosphorylated, MX2 is active, but when phosphorylated at these positions MX2 becomes inactive (Fig. 4d). MLCP therefore promotes MX2 anti-viral function by maintaining the unphosphorylated state of these serines. Critically, compromising MLCP function displays a consistent relationship with the impairment of MX2's anti-viral activity and increased phosphorylation of the S14-S17-S18 motif (Fig. 4d, e, f). That this pattern of regulation of viral inhibition was recapitulated with NTD-containing chimeric proteins (Supplementary Fig. 5a) points to an MX2 regulatory mechanism that is independent of other regions of MX2.

We also examined the consequences of serine phosphorylation for MX2's interactions with known ligands, with compromised binding to HIV-1 capsid (Fig. 5a), NUP214 and TNPO1 (Fig. 6c) being noted, further attesting to the relevance of dephosphorylation at these positions. Consistent with its loss of binding to NUP214/ TNPO1 and reminiscent of what has been described in cells depleted of both proteins²⁵, the inactive S14, 17-18D MX2 mutant displays reduced ability to accumulate at the nuclear envelope (Fig. 5b).

Our findings raise a number of key questions: principally, why is the activity of a potent IFN-induced anti-viral effector reversibly suppressed by serine phosphorylation? While answering this fully will require identification of the relevant kinase(s), we found that IFN treatment significantly reduces phosphorylation at the triple-serine motif (Fig. 6d, e). This opens the intriguing possibility that NTD phosphorylation is used as a "switch" to inactivate MX2 during basal conditions. Then, in the IFN-induced anti-viral state, MX2 is not only induced by transcription, but is also activated via NTD phosphorylation. In support of this model, we examined MX2-mediated inhibition of the nuclear import of non-viral cargo²⁶ and found that the import efficiency of a representative cellular NLS is impeded less efficiently by the S14,

17-18D mutant than by wild type MX2 (Fig. 6) – put differently, NTD serine phosphorylation limits its capacity to disrupt nucleocytoplasmic trafficking. Given that a naturally expressed short isoform of MX2 serves as competitive inhibitor of full length MX2²⁸, thus providing another mechanism for down-regulating MX2, we infer that effective balancing of MX2-mediated innate immunity with the preservation of normal cell function when MX2 is present at basal levels³ is of fundamental benefit to the host.

Methods

HIV-1 molecular clones and retroviral vectors

The HIV-1 NL4-3/Nef-IRES-Renilla reporter virus, wild type or P90A HIV-1 based lentiviral particles expressing GFP (HIV-1/GFP), MLV based retroviral particles expressing GFP (MLV/GFP), the pEasiLV inducible and IRES-puromycin N-acetyltransferase (puromycinR) lentiviral vector systems have been described previously^{3,13,24,25}. Retroviral based particles expressing GFP-LacZ fusion proteins have been described²⁶. Briefly, particles were produced by co-transfection of 293T cells with p5349, pMD.G and the specific GFP-LacZ construct plasmid at a ratio of 1:0.25:1, respectively. In all cases, transfections were performed using TransIT-2020 (Mirus) reagent at a 2:1 ratio with DNA. In all cases, culture medium was changed 24 h after transfection and again after a further 24 h, and filtered through 0.45 µm cut-off filters (Sartorius) to purify viral particles. Resulting media was either used stored at -80°C for future use (HIV/GFP, MLV/GFP and NL4-3/Nef-IRES-Renilla) or used immediately for transductions (pEasiLV, puromycinR and GFP-LacZ particles).

Cells

HeLa cells were obtained from Bryan Cullen. 293T cells were obtained from the American Type Culture Collection (ATCC). U87-MG CD4⁺ CXCR4⁺ cells, which stably express CD4 and CXCR4 have been described³. All cell lines were cultured in Dulbecco's modified Eagle medium (DMEM) supplemented with heat-inactivated foetal bovine serum (10%), L-glutamine, penicillin (100 U/ml) and streptomycin (100 µg/ml). Human primary CD4⁺ T cells were obtained from peripheral blood mononuclear cells (PBMCs) from healthy volunteer donors (approved by the Guy's Research Ethics Committee (Ref 03/02/06), and through the Infectious Diseases BioBank at King's College London (ethics reference MM2-220518) under overall permission from the Southampton and South West Hampshire Research Ethics Committee (B) (REC reference 19/SC/0232). CD4⁺ T cells were isolated from PBMCs using LymphoPrep (Axis-Shield) and the CD4⁺ T Cell Isolation Kit (Miltenyl Biotec) according

to the manufacturer's instructions. The purity of isolated cell populations was consistently over 90%, as determined by flow cytometric analysis of specific markers (CD4 and CD3) using anti-CD4 (BD Pharmingen, 555349) and anti-CD3 (BD Pharmingen, 555340) antibodies. Cells were activated by addition of Dynabeads Human T-Activator CD3/CD28 (ThermoFisher) and 50 U/ml recombinant IL-2 (rIL-2) (Roche) for 48 h in Roswell Park Memorial Institute (RPMI) 1640-GlutaMax medium, supplemented with 10% heat-inactivated autologous serum, penicillin (100 U/ml) and streptomycin (100 µg/ml). After activation, CD4⁺ T cells were further maintained in same medium containing 30 U/ml rIL-2. In some experiments, culture medium was supplemented with 500 or 2,000 U/ml IFNα-2b (INTRON A, Merck, Sharpe & Dohme Corp.).

siRNA mediated knock-down

Cultures of 50,000 U87-MG CD4⁺ CXCR4⁺ based cells were transfected twice, 24 h apart, with 10 nM of either smartpool siRNAs (Dharmacon) (for CTR (D-001210-03-05), MYPT1 (PPP1R12A) (M-011340-01-0005), PPP1CB (M-008685-00-0005) or MX2 (M-011736-01-0005)) or individual siRNAs (for MYPT1 (MQ-011340-01-0002) and PPP1CB (MQ-008685-00-0002)). In cases when IFNα was used, 8 h after the second transfection 500 U/ml IFNα was added to one dish of cells, while a second identical culture was left untreated. 24 h after IFNα addition, cells were challenged with HIV-1/GFP particles, and infectivity measured 48 h later by flow cytometry (FACSCalibur, BD Biosciences) (a representative example of the gating strategy used is displayed in Supplementary Fig. 7). The efficiency of knock-down was examined by immunoblot analysis of whole cell lysates harvested 32 h after the second siRNA transfection using anti-MYPT1 (Abcam, ab70809), anti-PPP1CB (Abcam, ab53315), anti-MX2 (Novus Biologicals, NBP1-81018) and anti-tubulin (Sigma, T5168).

Plasmids

cDNAs corresponding to MX1, MX2, MX2 R11-13A, GFP or GFP (NTD_{MX2}) were inserted into pCTAP-A (Agilent Technologies) to perform stable isotope labelling by amino acids (SILAC) analysis of MX2 interacting proteins. pEasiLV³ containing luciferase (Luc), wild type MX2, MX2 mutants or chimeric proteins (Fv1b (NTD_{MX2}) and MX1 (NTD_{MX2})) were produced by standard cloning or site directed mutagenesis. pEasiLV-BFP was obtained by substitution of the E2 crimson marker for blue fluorescent protein (BFP), and used for the insertion of DNAs encoding Luc, MYPT1 or PPP1CB. Wild type HIV-1 Capsid-Nucleocapsid (CANC, Gag residues 133-432), was cloned into pET-11a plasmid (Adgene). MX1, MX2 and MX2 S14, 17-18D were cloned into the puromycinR lentiviral vector replacing CD4 (Goujon, 2013). Retroviral based vectors expressing GFP-LacZ fusion proteins, as well as derivatives containing nuclear localization sequences (NLSs) for SV40 large T antigen, c-MYC, DDX21, *Xenopus laevis* NUPL, HnRNP K (KNS), HTLV-1 Rex or residues 1 to 25 of MX2 (N_{MX2}) were based on the retroviral LHCX vector and were kindly provided by Paul Bieniasz and Melissa Kane. Mutants NLS (N_{MX2}) S14, 17-18A-GFP-LacZ and NLS (N_{MX2}) S14, 17-18D-GFP-LacZ were obtained by site directed mutagenesis. pCAGGS vectors encoding Flag- or HA-tagged GFP, GFP (NTD_{MX2}), MX1, MX1 (NTD_{MX2}), MX2, C-terminal fragment (residues 1681-2080) of NUP214, TNPO1 or mutant derivatives have been described^{21,24,25}.

CRISPR-Cas9 knock-out cells

Control CRISPR U87-MG CD4⁺ CXCR4⁺ cells and MX2 CRISPR_1 clone have been described²⁵. MX2 CRISPR U87-MG CD4⁺ CXCR4⁺ bulk cells, as well as MX2 CRISPR_2 clone were generated using different specific guide RNAs targeting MX2 cloned into BsmBI-linearized lentiviral vector pLentiCRISPRv2^{44,45} using the oligonucleotides (forward/reverse) 5'-caccgGACAACCAGCCCCGAGACAT-3' and 5'-aaacATGTCTCGGGGCTGGTTGTCC-3'. Retroviral vectors expressing the guides were produced in 293T cells by transfection of HIV-1 packaging plasmid p8.91, vesicular stomatitis virus G (VSV-G) envelope vector (pMD.G) and pLentiCRISPRv2 at a ratio of 1.5:0.375:1.5, respectively. After transduction, U87-MG CD4⁺ CXCR4⁺ cells were selected for 72 h in the presence of 1 µg/ml puromycin (Sigma).

Single clone MX2 CRISPR_2 was derived from the bulk population by single-cell sorting in 96-well plates and the loss of MX2 confirmed by immunoblotting. MX2 gene disruption was validated by sequencing of the targeted genomic region (Genewiz).

shRNA-mediated silencing

CD4⁺ T cell gene silencing was achieved using a modified version of the HIV-1 based lentiviral vector pHRSIREN-S-SBP-ΔLNGFR-W where the antibody-free magnetic cell sorting selectable marker (SBP-ΔLNGFR) was replaced by E2-crimson^{9,25}. The shRNA targeting sequences for the negative control (scramble), MX2, PPP1CB and MYPT1, were 5'-GTTATAGGCTCGCAAAAGG-3', 5'-AAGATGTTCTTTCTAATTG-3', 5'-AGATTTGATTTGTCGAGCT-3' and 5'-GATGAAGAGTCTGAATCCC-3', respectively. Lentiviral vector stocks were obtained by co-transfection of 293T cells with pMD.G, p8.91 and pHRSIREN vector at a ratio of 0.5:1:1.5. After filtration, cell culture supernatants containing lentiviral particles were concentrated by ultracentrifugation at 28,000 x g for 75 min. Human primary CD4⁺ T cells were then transduced by spin-infection at 2,000 x g for 2 h at room temperature. Two days later, 3 x 10⁴ cells/well were seeded in 96 well plates in duplicates. 2,000 U/ml of IFN α was added to one of the wells, while the other was left untreated. 24 h later, cells were challenged with NL4.3/Nef-IRES-Renilla (measured as 30 ng p24^{Gag}) at 2,000 x g for 2 h at room temperature. Infection was left to proceed for 48 h, and infectivity levels were assessed by measuring Renilla luciferase activity using the Renilla Luciferase Assay System (Promega).

Quantification of mRNA expression

~10⁶ activated primary human CD4⁺ T cells treated or not for 24 h with 2,000 U/ml IFN α were collected and the RNA was extracted using the RNeasy Mini Kit (Qiagen). cDNA was produced using 500 ng of purified RNA and the High-Capacity cDNA Reverse Transcription Kit (Thermo Fisher). Quantitative PCR (qPCR) of selected genes was then performed using the following

TaqMan gene expression assays (Thermo Fisher): MYPT1 (Hs01552899), PPP1CB (Hs01027793), MX2 (Hs01550808) and GAPDH (Hs99999905). GAPDH was used to normalized expression levels.

Stable isotope labelling by amino acids (SILAC)

293T cells were grown in DMEM with no glutamine, no lysine, and no arginine (Thermo Fisher) supplemented with 10% dialyzed fetal bovine serum, 6 mM L-glutamine, 100 U/ml penicillin, 100 µg/ml streptomycin, containing either: a) 73 mg/l $^{13}\text{C}_6$ $^{15}\text{N}_2$ -L-lysine (Lys8) and 42 mg/l $^{13}\text{C}_6$ $^{15}\text{N}_4$ -L-arginine (Arg10) (CK Isotopes) for “heavy” conditions; b) 73 mg/l 4,4,5,5-D4-L-Lysine (Lys4) and 42 mg/l $^{13}\text{C}_6$ -L-arginine HCl (Arg6) (CK Isotopes) for “medium” conditions; c) 73 mg/l L-lysine (Lys0) and 42 mg/l L-arginine (Arg0) (Sigma) for “light” conditions. Cells were grown on the aforementioned media for at least two weeks prior to their use.

MX2 interacting proteins and mass spectrometry

For the identification of MX2 interacting proteins, groups of five 15 cm dishes of 293T cells variously labelled with “light”, “medium” or “heavy” arginine and lysine amino acids were transfected with 20 µg/dish of pCTAP-A vectors expressing either MX1, MX2, MX2 R11-13A, GFP or GFP (NTD_{MX2}), or empty vector. At 48 h, cells were lysed and over-expressed proteins isolated by streptavidin-affinity purification using the InterPlay Mammalian TAP System (Agilent Technologies) following the manufacturer’s instructions. Samples obtained from “light”, “medium” and “heavy” conditions were pooled together and resolved using 12% SDS-polyacrylamide gels and stained with SimplyBlue (Thermo Fisher). In-gel reduction, alkylation and trypsin digestion were subsequently conducted. Peptides were extracted from the gel by a series of washes of acetonitrile and water and subsequently lyophilised. Resulting samples were resuspended in 50 mM NH_4HCO_3 and analyzed by LC-MS/MS. Chromatographic separations were performed using an EASY nLC-II nanoflow system (Thermo Fisher). Reversed phase chromatography was used to resolve peptides, using a 75 µm C18 PepMap column and three step linear gradient of acetonitrile in CH_2O_2 (0.1%) at 300 nl/min. The eluate

was ionised by electrospray ionisation using an Orbitrap Velos Pro (Thermo Fisher, UK) operating under Xcalibur v2.2. The instrument was programmed to acquire in automated data-dependent switching mode, selecting precursor ions based on their intensity for sequencing by collision-induced fragmentation using a Top20 CID method. The MS/MS analyses were performed using collision energy profiles that were selected based on the mass-to-charge ratio (m/z) and the charge state of the peptide. Database searching was carried out using MaxQuant v1.4.3.14 (Max Planck Institute of Biochemistry) against the Uniprot human database. Parameters for single protein identification were set including cysteine carbamidomethylation as a fixed modification, with N-terminus acetylation and methionine oxidation as variable modifications. The minimum peptide length allowed was 7 and a maximum number of modifications per peptide of 5. Peptide-spectrum-matches and proteins were retained if they were below a false discovery rate of 1%. Additional analyses were conducted using Perseus software (version 1.4.1.3), obtaining sample relative abundance of identified proteins after removal of potential contaminants and reverse proteins. Illustrative pairwise comparisons are shown in Fig. 1a, though additional comparisons using different labels for the same protein pairs yielded similar results.

In experiments performed to study specific sites of MX2 phosphorylation, Flag-tagged immunoprecipitated protein samples from 293T cell lysates were reduced, alkylated and digested in-gel using Lys-C endoproteinase. The resulting peptides were re-suspended in 20 μ l sample solution (3% MeCN, 0.1% trifluoroacetic acid) and LC-MSMS data acquisition was performed on an Orbitrap Fusion Lumos (ThermoFisher) coupled to an RSLC3000 nanoHPLCs (ThermoFisher). The Fusion Lumos was configured with an EASYspray source using a 50 cm PepMap EASYspray emitter at 40°C. The nanoHPLC was operated with solvent A (0.1% CH_2O_2) and solvent B (80% MeCN, 0.1% CH_2O_2) at 250 nl/min with peptides resolved using a gradient rising from 3 to 40% solvent B by 60 min. MS data were acquired at 120k resolution between m/z 375 and 1500 with an AGC target of 4.0×10^5 . MS2 isolation was

performed in the quadrupole with HCD activation and 30% collision energy with fragment ions scanned in the Orbitrap at 30k resolution.

Data were processed in PEAKS 8 (Bioinformatics Solutions Inc., Ontario). A precursor mass error tolerance of 4.0 ppm and a fragment ion tolerance of 0.02 Da was used with a Uniprot Human database (downloaded 15/01/19), with the search performed using the default 485 built-in modifications.

Immunoprecipitation

Co-immunoprecipitations were conducted to confirm interactions between MX2 and endogenous PPP1CB or MYPT1, or ectopically expressed C-terminal fragment of NUP214 or TNPO1. 293T cells were seeded in 6-well plates and transfected singly with pCAGGs vectors expressing triple-HA tagged MX1, MX2 or MX2 R11-13A, or co-transfected with vectors expressing triple-HA tagged MX1, MX2 or MX2 S14, 17-18D and either pCAGGs vectors expressing Flag-tagged C-terminal fragment of NUP214 or TNPO1. At 48 h, cells were collected in lysis buffer (1x phosphate buffered saline, 0.5% Triton-X100, 1x complete protease inhibitor cocktail (Roche)) and lysed by sonication for 20 s. After lysate clarification for 10 min at 1500 x g and 4°C, a sample was withdrawn for analysis as input. Cell lysates were incubated with anti-HA magnetic beads (Pierce) for 2 h at 4 °C. Beads were then washed with lysis buffer 4 times before resuspension in sample buffer (200 mM Tris-HCl pH 6.8, 5.2% SDS, 20% glycerol, 0.1% bromophenol blue, 5% β-mercaptoethanol). HA- and Flag-tagged proteins were resolved using 12% SDS-polyacrylamide gels and detected by immunoblotting using anti-HA (Sigma, 12013819001) and anti-Flag (Sigma, A8592) antibodies.

To determine the phosphorylated residues in MX2, ten 15 cm dishes of 293T cells stably expressing Flag-tagged MX2 were obtained by transduction with puromycinR lentiviral vector and selection with 1.5 µg/ml of puromycin for 72 h. Cells were lysed in lysis buffer from the

InterPlay Mammalian TAP System (Agilent Technologies), supplemented with 1x PhosSTOP phosphatase inhibitor cocktail (Sigma) and 1x complete protease inhibitor cocktail (Roche). The resulting lysate was cleared by centrifugation at 16,000 x g for 10 min, and the supernatant was incubated with anti-Flag magnetic beads for 2 h at 4°C. The beads were washed 3 times with lysis buffer, resuspended in sample buffer and boiled for 10 min. Immunoprecipitated MX2 was resolved on a pre-cast 12% SDS-polyacrylamide gel (Thermo Fisher), stained with SimplyBlue (Thermo Fisher) and the band corresponding to MX2 excised for MS/MS analysis (see above).

Anti-phospho (P)-NTD MX2 antiserum production

The anti-P-NTD MX2 antiserum (AB2978) was generated using rabbits and a custom antibody production service (ThermoFisher). Sera were harvested 124 days after initial immunization with the C-PYRRR(pS)QF(pS)(pS)RK-amide peptide corresponding to amino acids 9 to 20 of MX2. The animals received four immunization boosts.

Immunoblotting

Cells were lysed in buffer containing 10 mM Tris-HCl pH 8, 150 mM NaCl, 1 mM EDTA, 1% Triton x-100 and 0.1% sodium deoxycholate. Lysates were briefly sonicated, boiled for 10 min and resolved in 12% SDS-polyacrylamide gels. After electrophoretically transferring proteins to a 0.45 µm nitrocellulose membrane (Amersham), their presence was analyzed using specific antibodies, described when required.

Immunofluorescence microscopy

HeLa or U87-MG CD4⁺ CXCR4⁺ cells stably expressing Flag-tagged wild type or mutant MX2 proteins, or MX1, were obtained by transduction with puromycinR lentiviral particles encoding the appropriate DNA and selection with 1 µg/ml puromycin for 72 h. Stable cells were seeded onto coverslips (treated with 0.01% poly-lysine (Sigma) in the case of U87-MG CD4⁺ CXCR4⁺ cells) at ~20,000 cells per well in 24-well plates. At 24 h, cells were washed three times with

1x phosphate buffer saline (PBS) and fixed in 4% paraformaldehyde (EM Sciences) for 15 min, before permeabilization with 0.2% Triton X-100 for 15 min. The specimens were blocked in buffer NGB (50 mM NH₄Cl, 2% goat serum, 2% bovine serum albumin) for 1 h. Flag-tagged proteins were detected using a mouse anti-Flag monoclonal M2 (Sigma, F3165) and secondary donkey anti-mouse antibody conjugated to Alexa 594 (Invitrogen, A-21203). Endogenous NUP358 was detected using rabbit anti-NUP358 polyclonal antibody (Abcam, ab64276) and secondary donkey anti-rabbit antibody conjugated to Alexa 488 (Invitrogen, A-21206). DAPI (4',6-diamidino-2-phenylindole) staining was used to demarcate the nucleus (0.1 mg/ml for 5 min).

Experiments conducted to address the behaviour of GFP-LacZ proteins bearing different NLSs have been described²⁶. Briefly, retroviral LHCX-based vectors containing different NLS-GFP-LacZ constructs were used to transduce HeLa cells. At 48 h, 600 µg/ml hygromycin (Invitrogen) was added for 5 days and hygromycin-resistant cells further transduced with puromycinR lentiviral particles expressing Flag-tagged MX1, MX2 or MX2 S14, 17-18D. 48 h later, puromycin-resistant cells were selected as described above, seeded on coverslips and subjected to immuno-staining. Cells were visualized using a Nikon A1 point-scanning laser confocal microscope (Nikon Instruments). Images were analyzed with ImageJ Fiji and the JACoP tool (Boltec and Cordelières, 2006). Quantification of the nuclear localization of wild type MX2 and MX2 S14, 17-18D was calculated as the percentage of total protein colocalizing with NUP358, using Manders' coefficient. In the case of the extent of nuclear localization of KNS-GFP-LacZ Manders' coefficient was used to quantify the colocalization with DAPI stain.

Drugs

Protein phosphatase inhibitors calyculin A (Abcam), okadaic acid (Enzo) and rubratoxin A (Abcam) were dissolved in DMSO. In all infectivity experiments, cells were treated with the desired drug concentration 6 h before infection (or DMSO as a negative control), and medium was changed 24 h after treatment.

Protein purification

CANC protein was expressed in *Escherichia coli* Rosetta (DE3) cells (Merck Millipore) as previously described⁴⁷. Briefly, 1 mM of isopropyl β -D-thiogalactopyranoside (IPTG) was used to induce protein expression for a total of 6 h at 30°C. Cell pellets were collected and sonicated until lysis was complete. Cell debris were removed by centrifugation for 20 min at 30,000 x g. The resulting supernatant was mixed with 0.11 volumes of 2 M $(\text{NH}_4)_2\text{SO}_4$ and the same volume of 10% polyethylenimine (PEI) pH 8.0 to remove nucleic acids. CANC was then precipitated by adding 0.35 volumes of saturated $(\text{NH}_4)_2\text{SO}_4$ and centrifugation at 10,000 x g for 10 min. Finally, pelleted protein was resuspended in 50 mM MES pH 6.5, 1 mM EDTA, 1 mM DTT, 0.5 M NaCl, 10% glycerol, 1 mM PMSF, CANC purified by cation-exchange chromatography and stored in 30 mM MES pH 6, 1 mM EDTA, 0.5 M NaCl, 10 mM DTT, and stored at -80°C.

CANC pull-down assays

Assembled CANC complexes were prepared by dilution of the protein to 40 μM final concentration in 50 mM Tris-HCl pH 8 containing 100 mM NaCl and adding 5 μM of TG50 oligonucleotide (5'- TG₍₂₅₎-3'). The reaction was incubated overnight at room temperature. For pull-down experiments, protein over-expression was achieved by transient transfection of 293T cells with relevant vectors. When used, siRNAs were transfected doubly, 24 h apart at a concentration of 10 nM. At 48 h after transfection, cells were lysed in hypotonic lysis buffer (10 mM Tris-HCl pH 8, 10 mM KCl, 1x complete protease inhibitor cocktail [Roche]) using a Dounce homogenizer. Cell lysates were cleared by centrifugation at 20,000 x g for 15 min at 4°C. 200 μl of the lysate was mixed with either 40 μl of Capsid assembly buffer (Cab, 50 mM Tris-HCl pH 8, 100 mM NaCl) containing 5 μM TG50 (as a control), or with 40 μl 40 μM of assembled CANC; an input sample was withdrawn from the latter. The mixtures were incubated for 1 h at room temperature, prior to overlay on a 250 μl 70% sucrose cushion.

Following centrifugation at 20,000 x g for 15 min at room temperature, a sample of the resulting supernatant was withdrawn, and the pellet washed with 500 µl of wash buffer (50 mM Tris-HCl pH 8, 50 mM NaCl and 5 mM KCl), and re-pelleted at 10,000 x g for 8 min. Finally, washed pellet was resuspended in 50 µl sample buffer. Input, supernatant and pellet fractions were analyzed by immunoblotting using anti-CA⁴⁸ and anti-Flag (Sigma, A8592) antibodies.

Quantification and statistical analysis

Statistical parameters in charts are expressed as means ± standard deviation (sd) for experimental replicates in each case, including the exact number of n. Differences between the experimental groups were evaluated, where indicated, by paired or unpaired two-tailed t-tests. Statistical significance in figures are denoted by asterisks (*p< 0.05, ns = not significant). In experiments analysing protein abundance by immunoblot, band intensities were quantified using Image J v1.51u software. Statistical analysis was performed in GraphPad PRISM 6 (Graph Pad software).

Data availability

For further information and requests for reagents, please contact the Lead Contact, Michael H. Malim (michael.malim@kcl.ac.uk). The plasmids generated in this study are available upon request without restriction.

Data and code availability

This study did not generate any unique datasets or code.

References

- 1 Doyle, T., Goujon, C. & Malim, M. H. HIV-1 and interferons: who's interfering with whom? *Nature Reviews Microbiology* **13**, 403-403 (2015).
- 2 Bourke, N. M. *et al.* Control of HIV infection by IFN- α : implications for latency and a cure. *Cellular and Molecular Life Sciences* **75**, 775-783 (2018).
- 3 Goujon, C. *et al.* Human MX2 is an interferon-induced post-entry inhibitor of HIV-1 infection. *Nature* **502**, 559-562 (2013).
- 4 Kane, M. *et al.* MX2 is an interferon-induced inhibitor of HIV-1 infection. *Nature* **502**, 563-566 (2013).
- 5 Liu, Z. *et al.* The interferon-inducible MxB protein inhibits HIV-1 infection. *Cell Host Microbe* **14**, 398-410 (2013).
- 6 Cramer, M. *et al.* MxB is an interferon-induced restriction factor of human herpesviruses. *Nat Commun* **9**, 1980-1980 (2018).
- 7 Schilling, M. *et al.* Human MxB protein is a pan-herpesvirus restriction factor. *J Virol* **92**, 17 (2018).
- 8 Staeheli, P. & Haller, O. Human MX2/MxB: a Potent Interferon-Induced Postentry Inhibitor of Herpesviruses and HIV-1. *Journal of Virology* **92**, 24 (2018).
- 9 Jimenez-Guardeño, J. M., Apolonia, L., Betancor, G. & Malim, M. H. Immunoproteasome activation enables human TRIM5 α restriction of HIV-1. *Nature Microbiology* (2019).
- 10 Wang, Y. X. *et al.* Interferon-inducible MX2 is a host restriction factor of hepatitis B virus replication. *J Hepatol*, (2019).
- 11 Matreyek, K. A. *et al.* Host and viral determinants for MxB restriction of HIV-1 infection. *Retrovirology* **11**, 90 (2014).
- 12 Busnadiego, I. *et al.* Host and Viral Determinants of Mx2 Antiretroviral Activity. *Journal of Virology* **88**, 7738-7752 (2014).

687 13 Bulli, L. *et al.* Complex Interplay between HIV-1 Capsid and MX2-Independent Alpha
688 Interferon-Induced Antiviral Factors. *J Virol* **90**, 7469-7480 (2016).

689 14 Staeheli, P., Haller, O., Boll, W., Lindenmann, J. & Weissmann, C. Mx protein:
690 Constitutive expression in 3T3 cells transformed with cloned Mx cDNA confers
691 selective resistance to influenza virus. *Cell* **44**, 147-158 (1986).

692 15 Gordien, E. *et al.* Inhibition of Hepatitis B Virus Replication by the Interferon-Inducible
693 MxA Protein. *Journal of Virology* **75**, 2684-2691 (2002).

694 16 Haller, O. & Kochs, G. Human MxA Protein: An Interferon-Induced Dynamin-Like
695 GTPase with Broad Antiviral Activity. *Journal of Interferon & Cytokine Research* **31**,
696 79-87 (2010).

697 17 Turan, K. *et al.* Nuclear MxA proteins form a complex with influenza virus NP and
698 inhibit the transcription of the engineered influenza virus genome. *Nucleic Acids*
699 *Research* **32**, 643-652 (2004).

700 18 Mitchell, P. S. *et al.* Evolution-guided identification of antiviral specificity determinants
701 in the broadly acting interferon-induced innate immunity factor MxA. *Cell Host Microbe*
702 **12**, 598-604 (2012).

703 19 Mänz, B. *et al.* Pandemic Influenza A Viruses Escape from Restriction by Human MxA
704 through Adaptive Mutations in the Nucleoprotein. *PLoS Pathogens* **9**, 3 (2013).

705 20 Patzina, C., Haller, O. & Kochs, G. Structural requirements for the antiviral activity of
706 the human MxA protein against Thogoto and influenza A virus. *Journal of Biological*
707 *Chemistry* **289**, 6020-6027 (2014).

708 21 Goujon, C. *et al.* Transfer of the Amino-Terminal Nuclear Envelope Targeting Domain
709 of Human MX2 Converts MX1 into an HIV-1 Resistance Factor. *Journal of Virology* **88**,
710 9017-9026 (2014).

711 22 Fricke, T. *et al.* MxB binds to the HIV-1 core and prevents the uncoating process of
712 HIV-1. *Retrovirology* **11**, 68-68 (2014).

713 23 Goujon, C., Greenbury, R. A., Papaioannou, S., Doyle, T. & Malim, M. H. A Triple-
714 Arginine Motif in the Amino-Terminal Domain and Oligomerization Are Required for
715 HIV-1 Inhibition by Human MX2. *Journal of Virology* **89**, 4676-4680 (2015).

716 24 Dicks, M. D. J. *et al.* Oligomerization Requirements for MX2-Mediated Suppression of
717 HIV-1 Infection. *Journal of Virology* **90** (2015).

718 25 Dicks, M. D. J. *et al.* Multiple components of the nuclear pore complex interact with the
719 amino-terminus of MX2 to facilitate HIV-1 restriction. *PLoS Pathogens* **14**, 1-24 (2018).

720 26 Kane, M. *et al.* Nuclear pore heterogeneity influences HIV-1 infection and the antiviral
721 activity of MX2. *eLife* **7**, 1-44 (2018).

722 27 Schulte, B. *et al.* Restriction of HIV-1 Requires the N-Terminal Region of MxB as a
723 Capsid-Binding Motif but Not as a Nuclear Localization Signal. *J Virol* **89**, 8599-8610
724 (2015).

725 28 Betancor, G. *et al.* The GTPase Domain of MX2 Interacts with the HIV-1 Capsid,
726 Enabling Its Short Isoform to Moderate Antiviral Restriction. *Cell Rep* **29**, 1923-1933
727 (2019).

728 29 Smaga, S. S. *et al.* MxB Restricts HIV-1 by Targeting the Tri-hexamer Interface of the
729 Viral Capsid. *Structure* **27**, 1234-1245 (2019).

730 30 Buffone, C., Schulte, B., Opp, S. & Diaz-Griffero, F. Contribution of MxB
731 oligomerization to HIV-1 capsid binding and restriction. *J Virol* **89**, 3285-3294 (2015).

732 31 Kiss, A., Erdődi, F. & Lontay, B. Myosin phosphatase: Unexpected functions of a long-
733 known enzyme. *BBA-Molecular Cell Research* **1866**, 2-15 (2019).

734 32 Heroes, E. *et al.* The PP1 binding code: A molecular-lego strategy that governs
735 specificity. *FEBS Journal* **280**, 584-595 (2013).

736 33 Wies, E. *et al.* Dephosphorylation of the RNA Sensors RIG-I and MDA5 by the
737 Phosphatase PP1 Is Essential for Innate Immune Signaling. *Immunity* **38**, 437-449
738 (2013).

739 34 Ishihara, H. *et al.* Calyculin A and okadaic acid: Inhibitors of protein phosphatase
740 activity. *Biochemical and Biophysical Research Communications* **159**, 871-877 (1989).

741 35 Takai, A. *et al.* Inhibitory effect of okadaic acid derivatives on protein phosphatases. A
742 study on structure-affinity relationship. *Biochemical Journal* **284**, 539-544 (2015).

743 36 Ammosova, T. *et al.* Nuclear targeting of protein phosphatase-1 by HIV-1 Tat protein.
744 *Journal of Biological Chemistry* **280**, 36364-36371 (2005).

745 37 Wada, S. I. *et al.* Rubratoxin A specifically and potently inhibits protein phosphatase
746 2A and suppresses cancer metastasis. *Cancer Science* **101**, 743-750 (2010).

747 38 Takai, A. *et al.* Protein phosphatases 1 and 2A and their naturally occurring inhibitors:
748 current topics in smooth muscle physiology and chemical biology. *J Physiol Sci* **68**, 1-
749 17 (2018).

750 39 Fribourgh, J. L. *et al.* Structural insight into HIV-1 restriction by MxB. *Cell Host and*
751 *Microbe* **16**, 627-638 (2014).

752 40 Melén, K. *et al.* Human MxB protein, an interferon- α -inducible GTPase, contains a
753 nuclear targeting signal and is localized in the heterochromatin region beneath the
754 nuclear envelope. *Journal of Biological Chemistry* **271**, 23478-23486 (1996).

755 41 Roy, J., Cyert, M. S. Cracking the Phosphatase Code- Docking Interactions Determine
756 Substrate Specificity. *Science Signaling* **2**, 100 (2009).

757 42 Grassie, M. E., Moffat, L. D., Walsh, M. P. & MacDonald, J. A. A regulated mechanism
758 for achieving substrate specificity of the catalytic subunit of protein phosphatase type
759 1 δ . *Archives of Biochemistry and Biophysics* **510**, 147-159 (2011).

760 43 Matsumura, F., Yamakita, Y. & Yamashiro, S. Myosin light chain kinases and
761 phosphatase in mitosis and cytokinesis. *Archives of Biochemistry and Biophysics* **510**,
762 76-82 (2011).

763 44 Sanjana, N. E., Shalem, O. & Zhang, F. Improved vectors and genome-wide libraries
764 for CRISPR screening. *Nature Methods* **11**, 783-784 (2014).

765 45 Shalem, O. *et al.* Genome-scale CRISPR-Cas9 knockout screening in human cells.
766 *Science* **343**, 84-87 (2014).

767 46 Bolte S. & Cordelières F.P. A guided tour into subcellular colocalization analysis in light
768 microscopy. *Journal of Microscopy* **224**, 213-232 (2006).

769 47 Schaller, T. *et al.* Effects of Inner Nuclear Membrane Proteins SUN1/UNC-84A and
770 SUN2/UNC-84B on the Early Steps of HIV-1 Infection. *J Virol* **91**, 19 (2017).
771 48 Fouchier, R. A., Meyer, B. E., Simon, J. H., Fischer, U. & Malim, M. H. HIV-1 infection
772 of non-dividing cells: evidence that the amino-terminal basic region of the viral matrix
773 protein is important for Gag processing but not for post-entry nuclear import. *EMBO J*
774 **16**, 4531-4539 (1997).
775

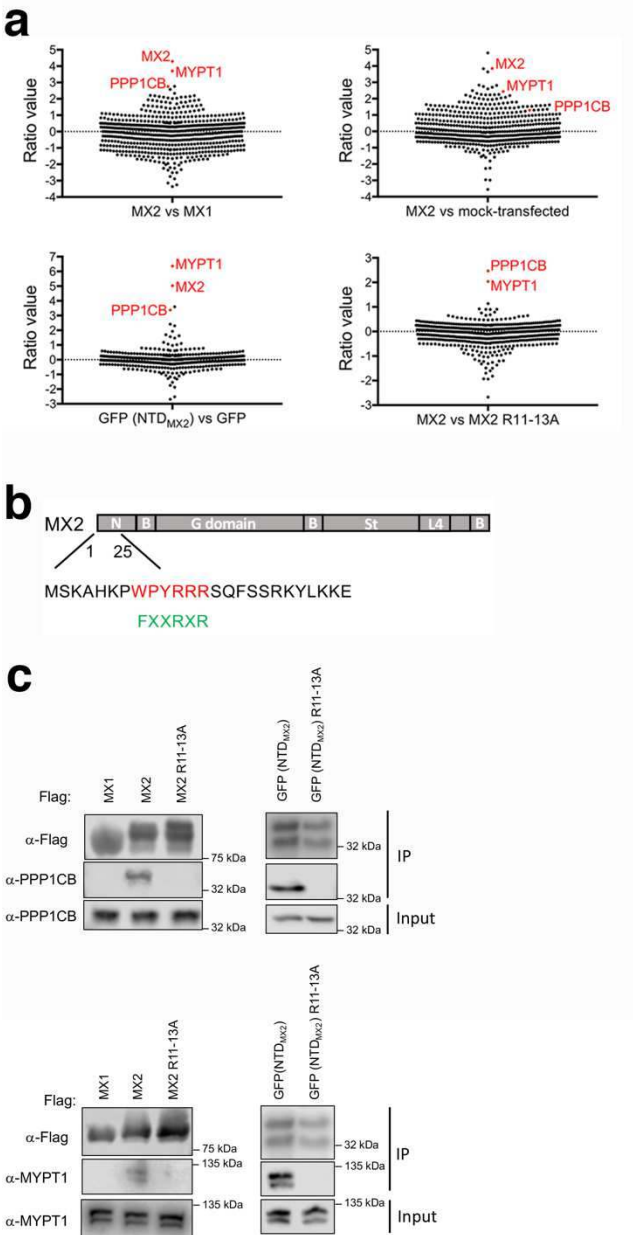


Fig. 1: The N-terminal domain of MX2 interacts with MYPT1 and PPP1CB

a, Stable isotope labelling by amino acids (SILAC) screen for MX2 binding proteins. Streptavidin-tagged MX2, MX1, MX2 R11-13A, GFP or GFP (NTD_{MX2}) were expressed in 293T cells labelled with “light”, “medium” or “heavy” amino acids, immune-affinity purified and analyzed by tandem mass spectrometry. Representative experiments comparing MX2 (medium) versus MX1 (light) (n= 3), MX2 (medium) versus mock (light) transfected cells (n=

786 1), GFP (NTD_{MX2}) (heavy) versus GFP (light) (n= 2) and MX2 (light) versus MX2 R11-13A
787 (medium) (n= 3) are shown. Values on the y-axis are in Log-2 scale.

788 **b**, MX2 domain organization showing the sequence of the N-terminal 25 amino acids,
789 highlighting the MLCP binding motif (in red) and a consensus PP1 binding sequence (in
790 green).

791 **c**, Interaction of endogenous PPP1CB (upper panel) or MYPT1 (lower panel) with the MX2 N-
792 terminal domain. Transfected 293T cells expressing Flag-tagged MX1, MX2, MX2 R11-13A,
793 GFP (NTD_{MX2}) or GFP (NTD_{MX2}) R11-13A were lysed, proteins immunoprecipitated (IP) with
794 an anti-Flag antibody and analyzed by immunoblot using anti-PPP1CB, anti-MYPT1 or anti-
795 Flag antibodies. All experiments were done at least 4 times.

796

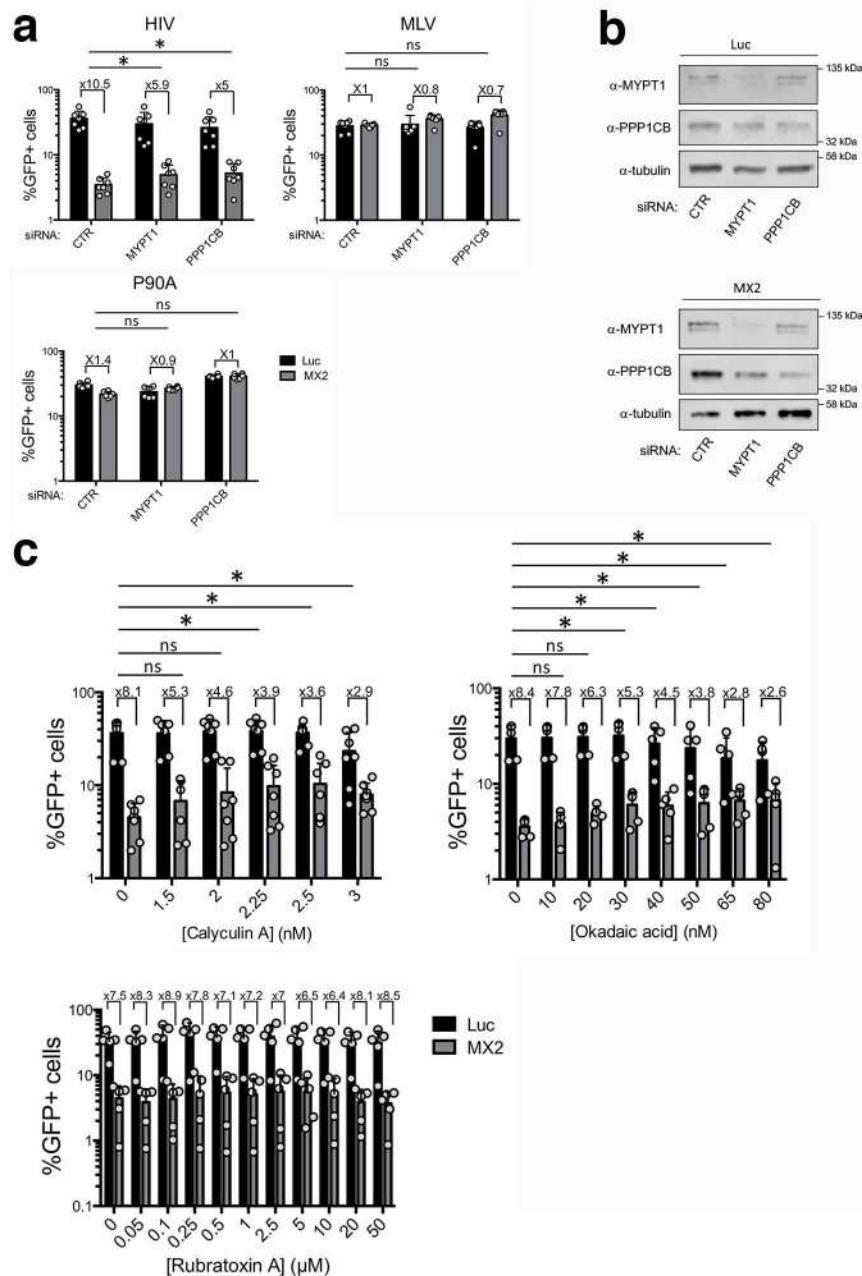


Fig. 2: MX2 requires functional MLCP for anti-viral activity

a, U73-MG CD4⁺ CXCR4⁺ cells were transduced with pEasiLV vectors expressing MX2 or the negative control protein Luc and protein expression induced by doxycycline (0.5 μg/ml) for 48 h. MYPT1 or PPP1CB were then depleted by double siRNA transfection. Cells were challenged with wild type or P90A versions of HIV-1/GFP or MLV/GFP and the percentage of infected cells from the pEasiLV transduced population (typically >85%), enumerated at 48 h

805 by flow cytometry (n = at least 6, mean \pm standard deviation (SD) *p value <0.05; two-tailed
806 unpaired *t*-test).

807 **b**, Immunoblot analysis of MYPT1 and PPP1CB depletion in U87-MG CD4⁺ CXCR4⁺ cells
808 from panel A. Tubulin is included as a loading control.

809 **c**, U87-MG CD4⁺ CXCR4⁺ cells expressing MX2 or Luc were treated with increasing
810 concentrations of calyculin A, okadaic acid or rubratoxin A (or DMSO as a control) 6 h before
811 challenge with HIV-1/GFP. Inhibitors were removed 24 h after addition and the percentage of
812 infected cells enumerated at 48 h by flow cytometry (n = at least 4, mean \pm SD, *p value <0.05,
813 (ns) non-significant; two-tailed unpaired *t*-test).

814

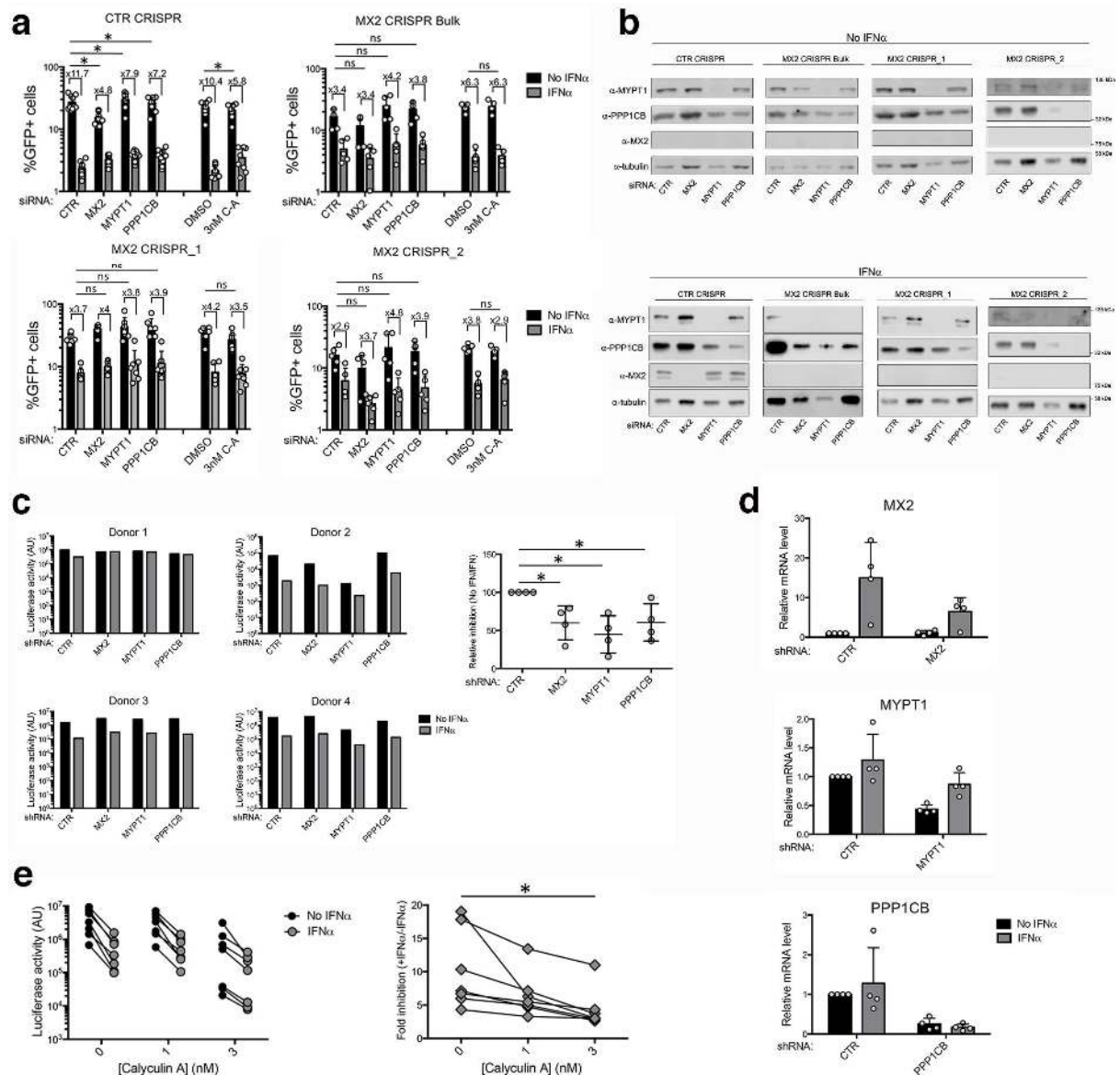


Fig. 3: Lack of functional MLCP diminishes MX2-mediated inhibition of HIV-1 infection during the IFN response

a, U87-MG CD4⁺ CXCR4⁺ cells transduced with a CRISPR-Cas9 control guide RNA, as well as a bulk population and two clonal cell lines where MX2 alleles had been disrupted by CRISPR-Cas9 genome editing, were either transfected twice with a control siRNA (CTR), or siRNAs targeting MX2, MYPT1 or PPP1CB, and treated or not with 500 U/ml IFN α for 24 h. Alternatively, cells were treated with 3 nM calyculin A (or DMSO) 6 h before infection and medium exchange 18 h later. Cells were challenged with HIV-1/GFP and infection enumerated

at 48 h by flow cytometry (n = at least 5, mean \pm SD, *p value <0.05; two-tailed unpaired *t*-test).

b, Immunoblot analysis of MX2, MYPT1, PPP1CB and tubulin (loading control) in CTR CRISPR, MX2 CRISPR Bulk, MX2 CRISPR_1 and MX2 CRISPR_2 cells in the presence or absence of IFN α , and transfected with siRNAs (from panel A).

c, Primary CD4⁺ T cells were isolated from 4 independent donors, transduced with shRNAs targeting MX2, MYPT1, PPP1CB or a scrambled sequence shRNA (CTR) and treated or not with 2,000 U/ml IFN α . At 24 h, cells were challenged with NL4.3/Nef-IRES-Renilla and luciferase activity determined 48 h later. Raw infectivity data are shown for each donor on the left (mean values from 3 technical replicates), and the fold inhibition of infection (no IFN/IFN) normalized to the CTR shRNA (assigned an arbitrary value of 100), on the right (*p-value <0.05; two-tailed paired *t*-test).

d, Efficiency of MX2, MYPT1 or PPP1CB depletion in primary CD4⁺ T cells after shRNA transduction was quantitated by qPCR in the presence or absence of IFN α , normalizing to GAPDH. Data shown represent the 4 donors used in panel C.

e, Primary CD4⁺ T cells isolated from 7 independent donors and treated or not with 2,000 U/ml of IFN α were incubated in the presence of DMSO or two concentrations of calyculin A (1 nm or 3 nM). After 6 h, cells were challenged with NL4.3/Nef-IRES-Renilla, the medium replaced 18 h later, and luciferase activity determined 48 h after infection. Raw infectivity data from all 7 donors are shown on the left and the fold inhibition of infection (no IFN/IFN), on the right (*p-value <0.05; two-tailed paired *t*-test).

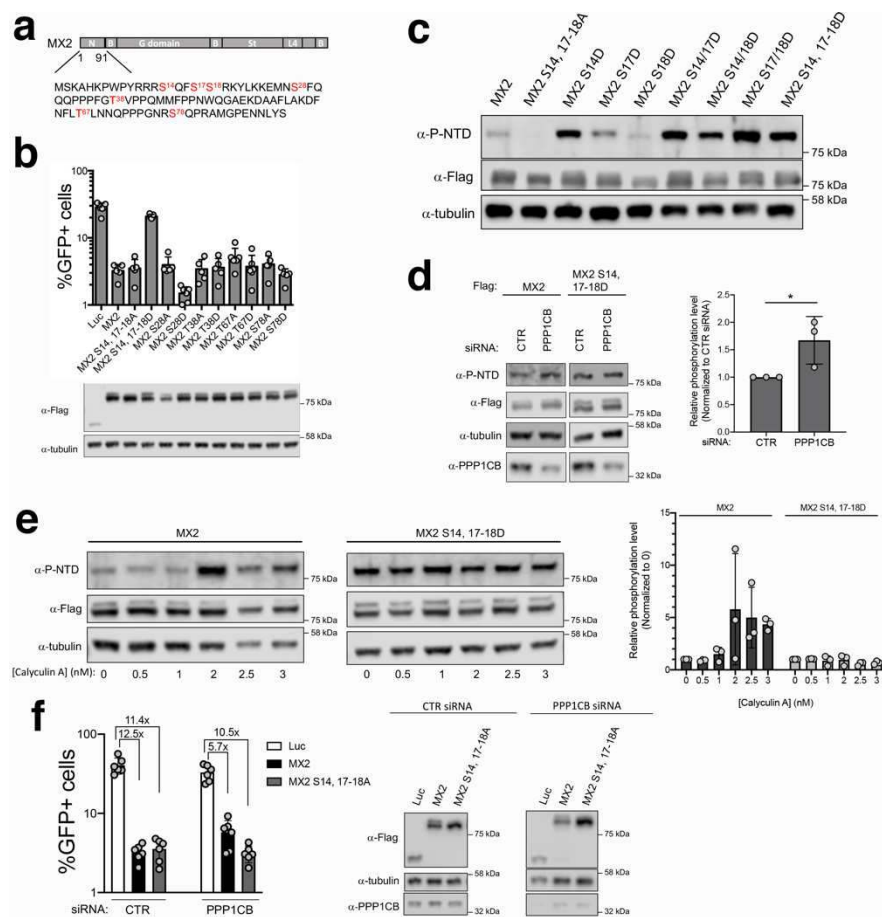


Fig. 4: MX2 anti-viral activity is antagonized by phosphorylation

a, MX2 domain organization showing the sequence of the N-terminal domain, and indicating residues found to be phosphorylated (in red).

b, U87-MG CD4⁺ CXCR4⁺ cells were transduced with pEasiLV expressing Flag-tagged wild type or mutant MX2, or the Luc control. After induction with 0.5 µg/ml of doxycycline for 48 h, cells were challenged with HIV-1/GFP and infectivity measured 48 h later (n = 5, mean ± SD). The anti-Flag immunoblot shows MX2 expression levels, with tubulin as the loading control.

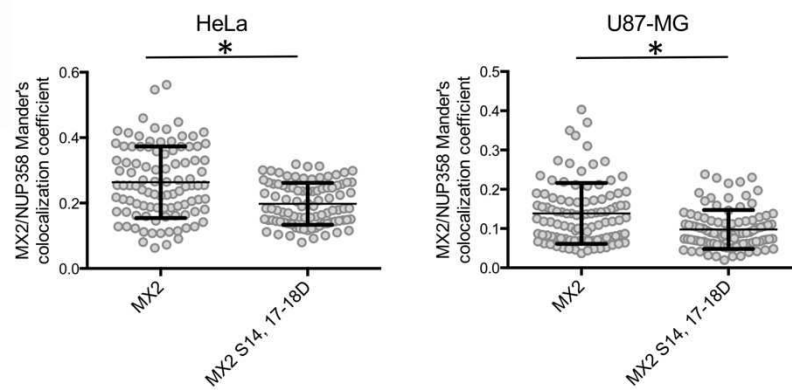
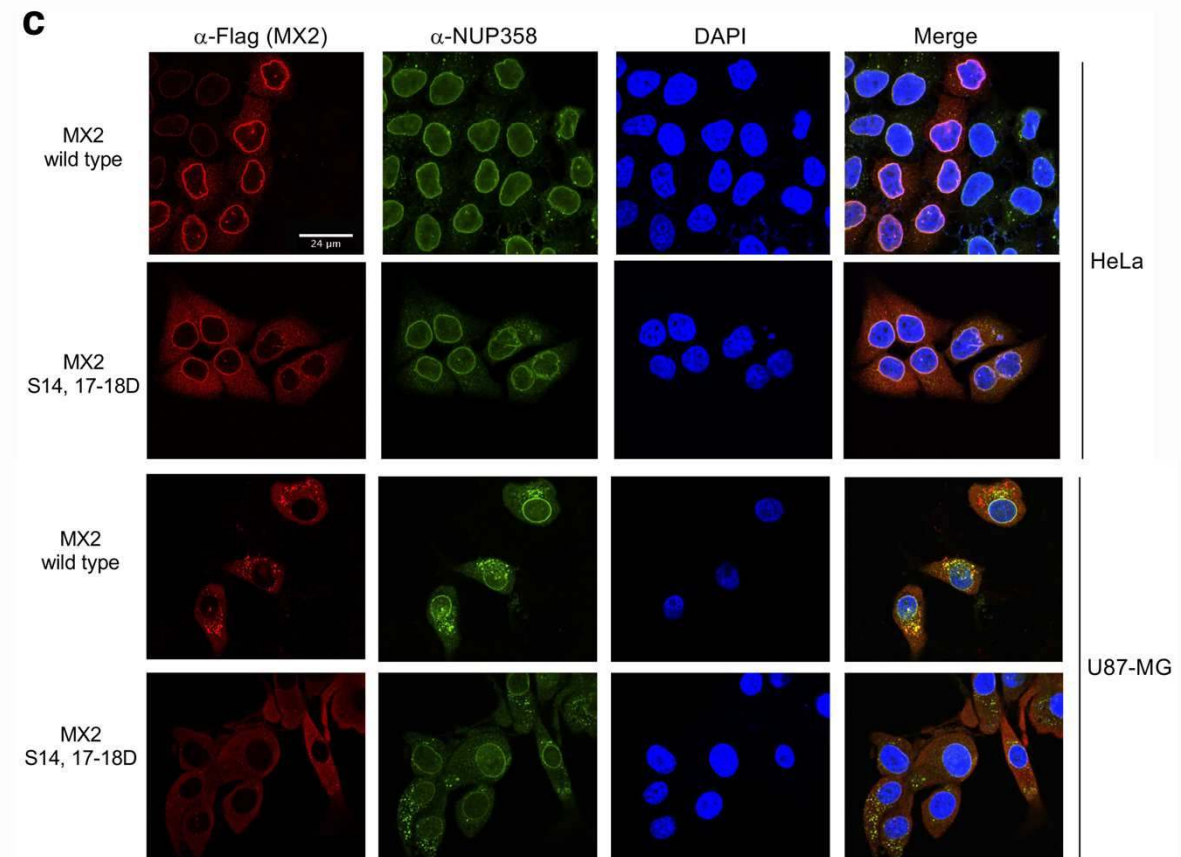
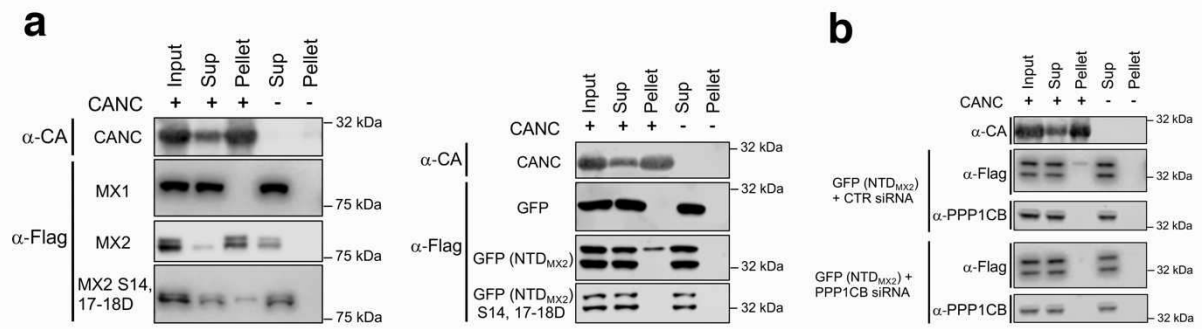
c, Specificity of the anti-phosphorylated S14, 17-18 NTD antibody (anti-P-NTD) was defined using lysates from U87-MG CD4⁺ CXCR4⁺ cells expressing wild type or mutated MX2 proteins. Total protein expression (anti-Flag) is shown with tubulin serving as a loading control.

d, MX2 or MX2 S14, 17-18D expressing U87-MG CD4⁺ CXCR4⁺ cells were doubly transfected with a siRNA targeting PPP1CB or a siRNA CTR. 48 h after the first transfection cells were

lysed and the levels of MX2 phosphorylated at the S14-S17-S18 motif (anti-P-NTD), total MX2 (anti-Flag) or PPP1CB determined by immunoblot. Tubulin was used as a loading control. Quantification of the level of phosphorylation, relative to the MX2 long isoform, and normalized to the CTR siRNA, is shown on the right (n = 3, mean \pm SD, *p value <0.05; two-tailed unpaired *t*-test).

e, DMSO (0) or increasing concentrations of calyculin A were used to inhibit MLCP in U87-MG CD4⁺ CXCR4⁺ cells expressing MX2 or MX2 S14, 17-18D. 6 h after treatment, cells were lysed and the levels of MX2 (anti-Flag), MX2 phosphorylated at the S14-S17-S18 motif (anti-P-NTD) or PPP1CB determined by immunoblot. Tubulin was used as a loading control. Quantification of the level of phosphorylation, relative to the MX2 long isoform, and normalized to the DMSO control condition, is shown on the right (n = 3, mean \pm SD, *p value <0.05; two-tailed unpaired *t*-test).

f, U87-MG CD4⁺ CXCR4⁺ cells expressing Luc, MX2 or MX2 S14, 17-18A were transfected with a CTR siRNA or a siRNA targeting PPP1CB before being challenged with HIV-1/GFP and infectivity measured 48 h later by flow cytometry (n = 6, mean \pm SD). The fold inhibition by MX2 species, relative to Luc, is also shown. Fold inhibition for MX2 is significantly lower in PPP1CB siRNA treated cells compared to CTR siRNA treated cells (12.5x vs 5.7x; p value <0.05; two-tailed unpaired *t*-test), but not for MX2 S14, 17-18A (11.4x vs 10.5x). Protein expression was confirmed by immunoblot (right panel).



881

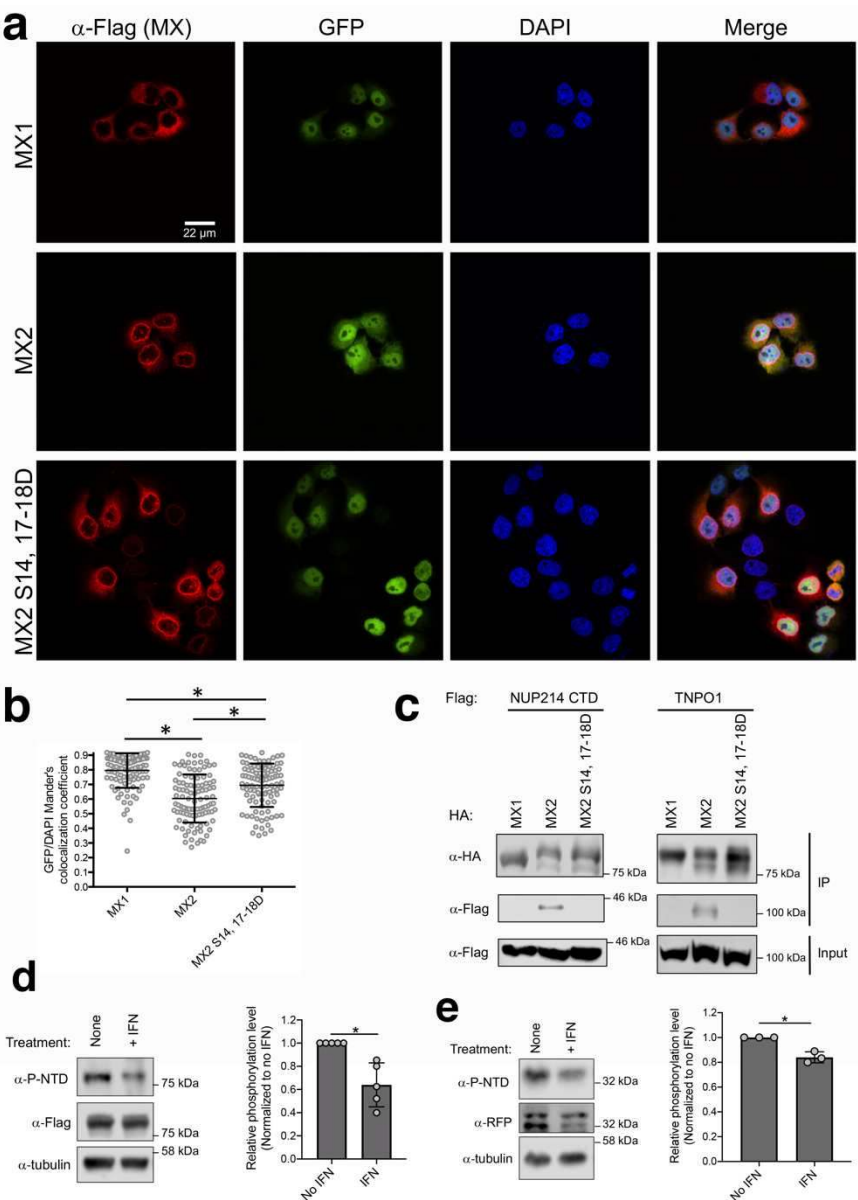
882

Fig. 5: Phosphorylation of residues 14, 17 and 18 inhibits the interaction of MX2 with the HIV-1 capsid and modulates its accumulation at the nuclear envelope

a, 293T cells were transfected with pCAGGs vectors expressing Flag-tagged MX1, MX2, mutant MX2 S14, 17-18D, GFP, GFP (NTD_{MX2}) or GFP (NTD_{MX2}) S14, 17-18D. Cell lysates were incubated in the presence or absence of Capsid-Nucleocapsid (CANC) assemblies and subjected to centrifugation through a sucrose cushion. Supernatant (Sup) and Pellet fractions, together with the Input sample, were analyzed by immunoblot using an anti-Flag antibody. A representative immunoblot for CANC (anti-CA) is shown. All experiments were done at least 4 times.

b, 293T cells expressing GFP (NTD_{MX2}) were transfected twice with a CTR siRNA or siRNA targeting PPP1CB, lysed and incubated with CANC assemblies. The resulting mixture was centrifuged through a sucrose cushion and resulting Sup and Pellet fractions, together with an Input sample, were analyzed by immunoblot using an anti-Flag antibody. A representative immunoblot for CANC (anti-CA) is shown. The efficiency of PPP1CB depletion was confirmed by immunoblot using an anti-PPP1CB antibody. All experiments were done at least 3 times.

c, HeLa and U87-MG CD4⁺ CXCR4⁺ cells stably expressing wild type or S14, 17-18D mutant MX2 bearing a C-terminal Flag-tag were seeded onto glass coverslips. Localization of MX2, and endogenous NUP358 (a marker for the nuclear envelope) were determined by fluorescence confocal microscopy using anti-Flag and anti-NUP358 antibodies, respectively. DAPI was used to stain the nuclei. Below, colocalization of MX2 and NUP358 was quantified using Mander's coefficient for an average of 97 cells per condition, randomly selected (*p-value <0.05; two-tailed unpaired *t*-test)



907

908 **Fig. 6: Phosphorylation of MX2 regulates interference with the nuclear import of cellular**
909 **cargo**

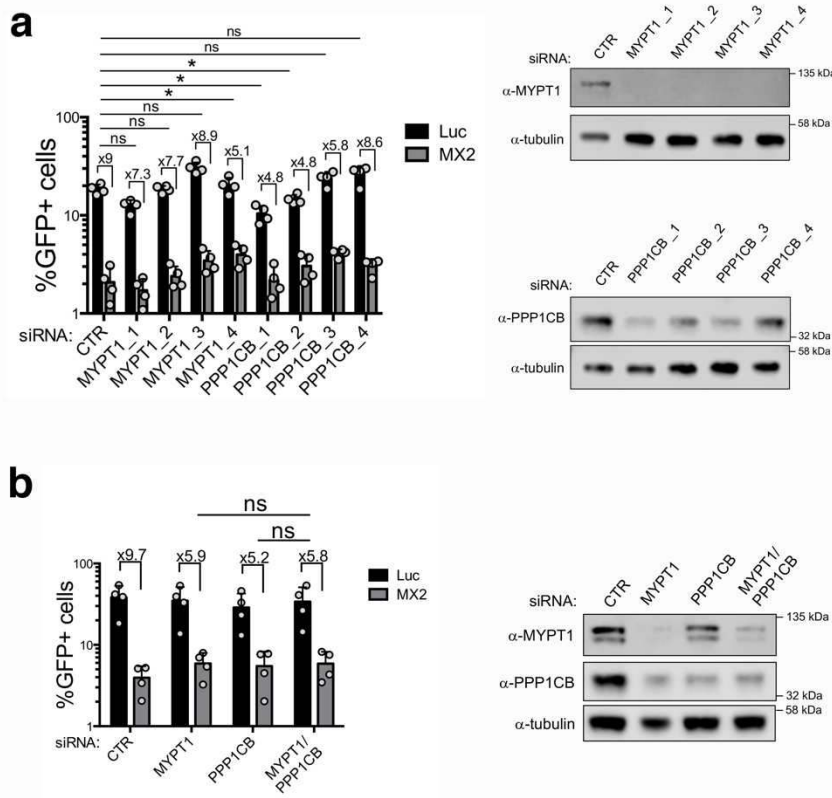
910 **a**, HeLa cells stably expressing the HNRNP K (KNS)-GFP-LacZ chimera were transduced
911 with puromycinR vectors expressing Flag-tagged MX1, MX2 or MX2 S14, 17-18D and
912 selected for 48 h with puromycin before seeding on glass coverslips. MX proteins were
913 detected using an anti-Flag antibody and the nuclei were stained with DAPI.

b, Nuclear localization of KNS-GFP-LacZ was determined for single cells by quantifying colocalization with DAPI using Mander's coefficient for an average of 104 randomly selected cells (*p-value <0.05; two-tailed unpaired *t*-test).

c, 293T cells were co-transfected with vectors expressing HA-tagged MX1, MX2 or S14, 17-18D MX2 and Flag-tagged TNPO1 or a C-terminal fragment of NUP214. Cells were lysed and HA-tagged proteins immunoprecipitated and analyzed (together with input samples) by immunoblot using anti-Flag and anti-HA antibodies. All experiments were performed at least 3 times.

d, U87-MG CD4⁺ CXCR4⁺ cells stably expressing Flag-tagged MX2 were treated or not with 1000 U/ml IFN α for 24 h before lysis and immunoblot analysis with anti-P-NTD or anti-Flag antibodies. Tubulin was used as a loading control. The level of MX2 phosphorylated at the S14-S17-S18 motif, relative to the MX2 long isoform, and normalized to the untreated condition was determined (n =5, mean \pm SD, *p-value <0.05; two-tailed unpaired *t*-test).

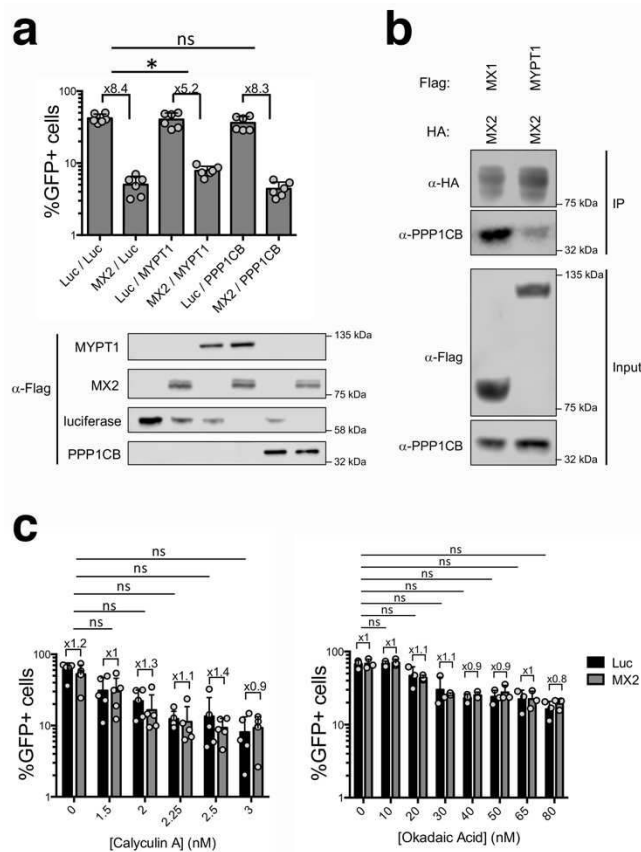
e, RFP bearing the NTD of MX2 (RFP(NTD_{MX2})) was expressed in U87-MG CD4⁺ CXCR4⁺ cells. Cells were incubated or not with 1000 U/ml IFN α for 24 h, lysed and the level of phosphorylation at the S14-S17-S18 motif, relative to the RFP (NTD_{MX2}) long isoform and normalized to the untreated condition, determined as in panel d (n =3, mean \pm SD, *p-value <0.05; two-tailed unpaired *t*-test).



Supplementary Fig. 1: Effect of MYPT1 and PPP1CB depletion on MX2-mediated inhibition of HIV-1.

a, Individual siRNAs targeting MYPT1 or PPP1CB, as well as a CTR siRNA were used to transfect U87-MG CD4⁺ CXCR4⁺ cells expressing MX2 or Luc. 48 h after challenging with HIV-1/GFP, infectivity was determined by flow cytometry (n = 4 mean ± SD, *p-value < 0.05, (ns) non-significant; two-tailed unpaired *t*-test). Immunoblot analyses to the right demonstrate the extents of reductions in protein levels.

b, U87-MG CD4⁺ CXCR4⁺ cells were transduced with pEasiLV expressing Luc or MX2 and pretreated with doxycycline for 48 h before being doubly transfected with CTR siRNA or siRNAs targeting MYPT1 and/or PPP1CB. Levels of HIV-1/GFP infectivity were determined by flow cytometry at 48 h (n = 4, mean ± SD, (ns) non-significant; two-tailed unpaired *t*-test). Immunoblot analyses to the right demonstrate the extents of reductions in protein levels.



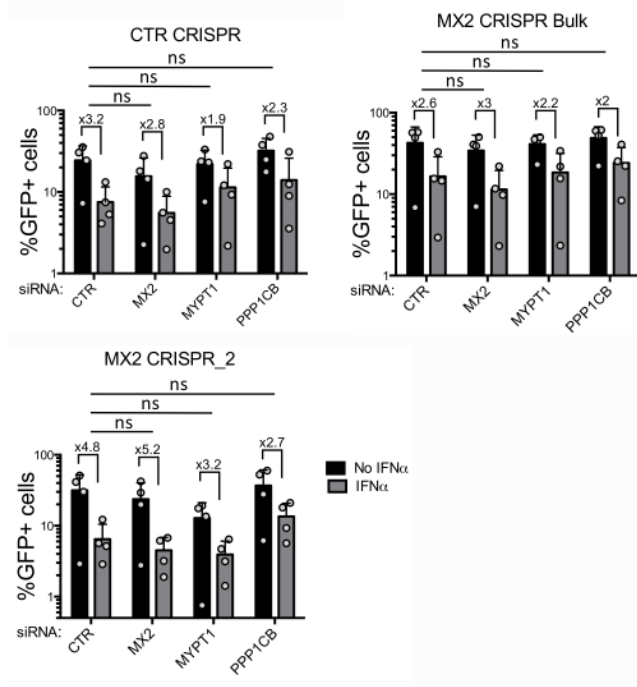
Supplementary Fig. 2: Role of functional MLCP in viral infection.

a, U87-MG CD4⁺ CXCR4⁺ cells were doubly transduced with pEasiLV expressing Flag-tagged Luc or MX2 and also with pEasiLV-BFP expressing Flag-tagged Luc, MYPT1 or PPP1CB. Infectivity data with HIV-1/GFP are shown (above) and immunoblotting was used to determine the expression of each construct (below) (n = 6, mean ± SD, *p-value <0.05, (ns) non-significant; two-tailed unpaired *t*-test).

b, 293T cells doubly transfected with pCAGGs plasmids expressing HA-tagged MX2 and either Flag-tagged MX1 or Flag-tagged MYPT1 were lysed, MX2 was immunoprecipitated using an anti-HA antibody and recovered proteins analyzed by immunoblot using anti-PPP1CB, anti-HA or anti-Flag antibodies. All experiments were done at least 4 times.

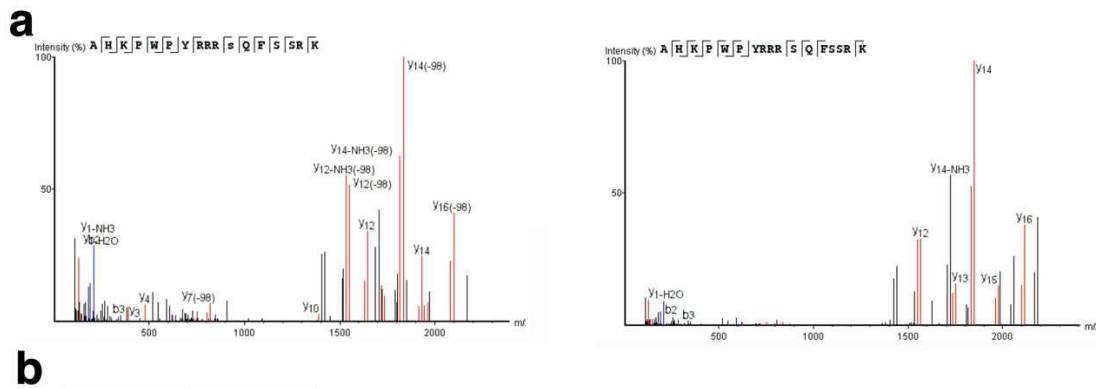
c, Titration of calyculin A and okadaic acid in U87-MG CD4⁺ CXCR4⁺ expressing Luc or MX2 and challenged with MLV/GFP. The number of infected cells was determined by enumeration

963 of GFP expressing cells by flow cytometry 48 h after challenging (n = at least 3, mean \pm SD,
964 (ns) non-significant; two-tailed unpaired *t*-test).
965



Supplementary Fig. 3: MX2, MYPT1 and PPP1CB do not participate in IFN-mediated suppression of MLV infection.

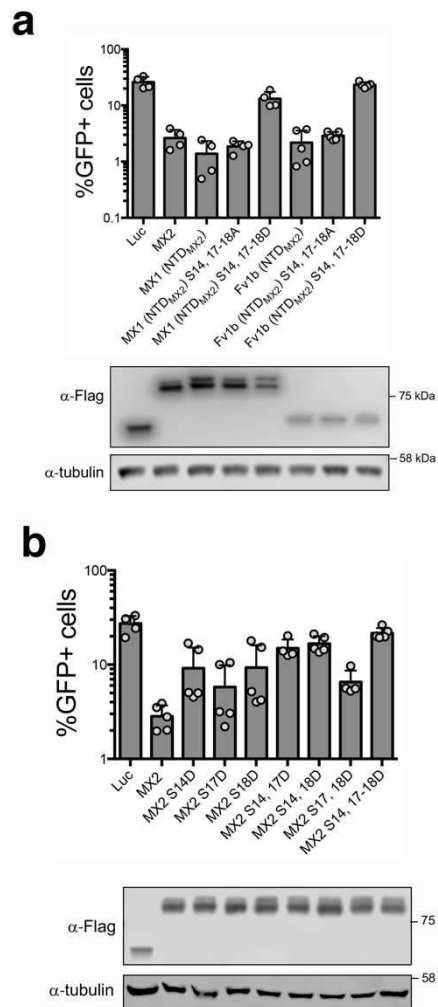
U87-MG CD4⁺ CXCR4⁺ cells depleted of MX2 using CRISPR-Cas9 genome editing (bulk population and clone MX2 CRISPR_2) and CTR CRISPR cells were transduced with pEasiLV expressing Luc or MX2, incubated in the presence or absence of 500 U/ml IFN α , and challenged with MLV/GFP. Infectivity was determined 48 h later by flow cytometry (n = 4, mean \pm SD, (ns) non-significant; two-tailed unpaired *t*-test).



Supplementary Fig. 4: Phosphorylation of MX2.

a, Example of LC-MSMS data from LysC generated MX2 peptides spanning A4 to K20, acquired on an Orbitrap Lumos and processed in PEAKS 8. The spectrum on the left shows the unphosphorylated form of the peptide and the spectrum on the right shows the corresponding peptide with putative phosphorylation at S14.

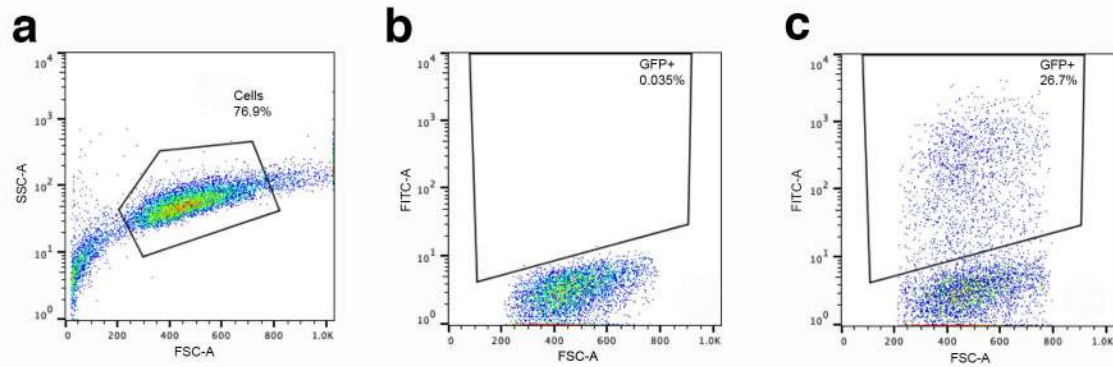
b, 293T cells expressing C-terminally Flag-tagged MX2 were treated with 3 nM calyculin-A. After 6 h, cells were lysed, MX2 immunoprecipitated and the resulting protein digested with LysC. LC-MSMS data were processed in PEAKS 8. Sum peak areas for peptides spanning from M1 to K20 and covering serines 14, 17 and 18 were calculated using the areas under the curves, where the x-axis represents time and the y-axis represents intensity.



Supplementary Fig. 5: Phosphorylation of serines 14, 17 and 18 antagonizes the anti-viral activity of MX2.

a, Residues S14, S17 and S18 in the N-terminal domain of the chimeras MX1 (NTD_{MX2}) or Fv1b (NTD_{MX2}) were substituted for alanine or aspartic acid and the effects on HIV-1/GFP infectivity measured at 48 h by flow cytometry (n = at least 4, mean ± SD). Protein expression was confirmed by immunoblot.

b, Residues 14, 17 and 18 of Flag-tagged MX2 were substituted for aspartic acid individually, in pairs or in triplicate. U87-MG CD4⁺ CXCR4⁺ cells expressing Luc, wild type or mutant proteins were challenged with HIV-1/GFP and infectivity was determined at 48 h by flow cytometry (n = 5, mean ± SD). Below, immunoblot showing protein expression.



Supplementary Fig. 6: Gating strategy for flow cytometry analysis of GFP+ infected cells.

a, Cells were distinguished from debris using the forward scatter (FCS, related to the cell size) and side scatter (SSC, related to the cell granularity).

b, Selected population was gated for GFP+ (FITC channel) using uninfected cells as negative control.

c, HIV-1/GFP infected cells were then gated for GFP. A representative plot showing GFP+ cells is shown.

Acknowledgments We thank Darja Pollpeter, Leandro Ventimiglia, Stelios Papaioannou, Paul Lehner, John Cason, Christine Mant, Melissa Kane and Paul Bieniasz for the provision of reagents and helpful discussions. The work was supported by the Wellcome Trust (106223/Z/14/Z), the Medical Research Council (MR/M001199/1), the National Institutes of Health (U54 GM103368, AI150472) and the Department of Health via a National Institute for Health Research comprehensive Biomedical Research Centre award to Guy's and St. Thomas' NHS Foundation Trust in partnership with King's College London and King's College Hospital NHS Foundation Trust. J.M.J.-G. is a Long-Term Fellow of the European Molecular Biology Organization (EMBO) (ALTF 663-2016).

Author contributions GB and MHM designed the study and wrote the manuscript with input from all co-authors; GB carried out the experiments and analyzed the data, with contributions from AES in figure 1, MDJD in figure 2, JMJ-G in figure 3, 5 and figure S2, SL in figure 1 and RA in figure 4; AES, MDJD and JMJ-G contributed to the execution of experiments and provided reagents; and, MHM supervised all aspects of the project.

Conflict of interest The authors declare that they have no conflict of interest.

Figures

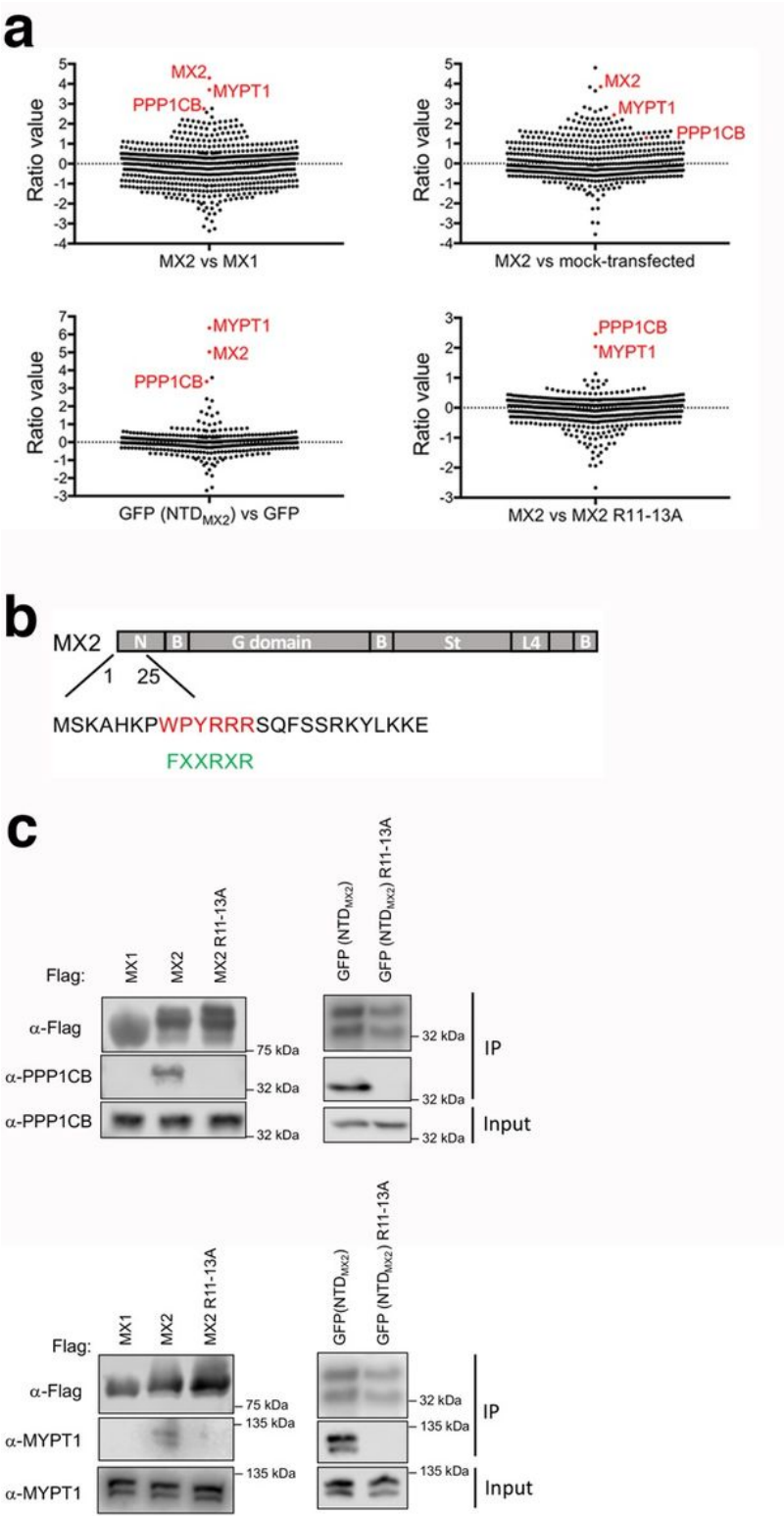


Figure 1

The N-terminal domain of MX2 interacts with MYPT1 and PPP1CB a, Stable isotope labelling by amino acids (SILAC) screen for MX2 binding proteins. Streptavidin-tagged MX2, MX1, MX2 R11-13A, GFP or GFP (NTDMX2) were expressed in 293T cells labelled with “light”, “medium” or “heavy” amino acids, immune-

affinity purified and analyzed by tandem mass spectrometry. Representative experiments comparing MX2 (medium) versus MX1 (light) (n= 3), MX2 (medium) versus mock (light) transfected cells (n=1), GFP (NTDMX2) (heavy) versus GFP (light) (n= 2) and MX2 (light) versus MX2 R11-13A (medium) (n= 3) are shown. Values on the y-axis are in Log-2 scale. b, MX2 domain organization showing the sequence of the N-terminal 25 amino acids, highlighting the MLCP binding motif (in red) and a consensus PP1 binding sequence (in green). c, Interaction of endogenous PPP1CB (upper panel) or MYPT1 (lower panel) with the MX2 N terminal domain. Transfected 293T cells expressing Flag-tagged MX1, MX2, MX2 R11-13A, GFP (NTDMX2) or GFP (NTDMX2) R11-13A were lysed, proteins immunoprecipitated (IP) with an anti-Flag antibody and analyzed by immunoblot using anti-PPP1CB, anti-MYPT1 or anti- Flag antibodies. All experiments were done at least 4 times.

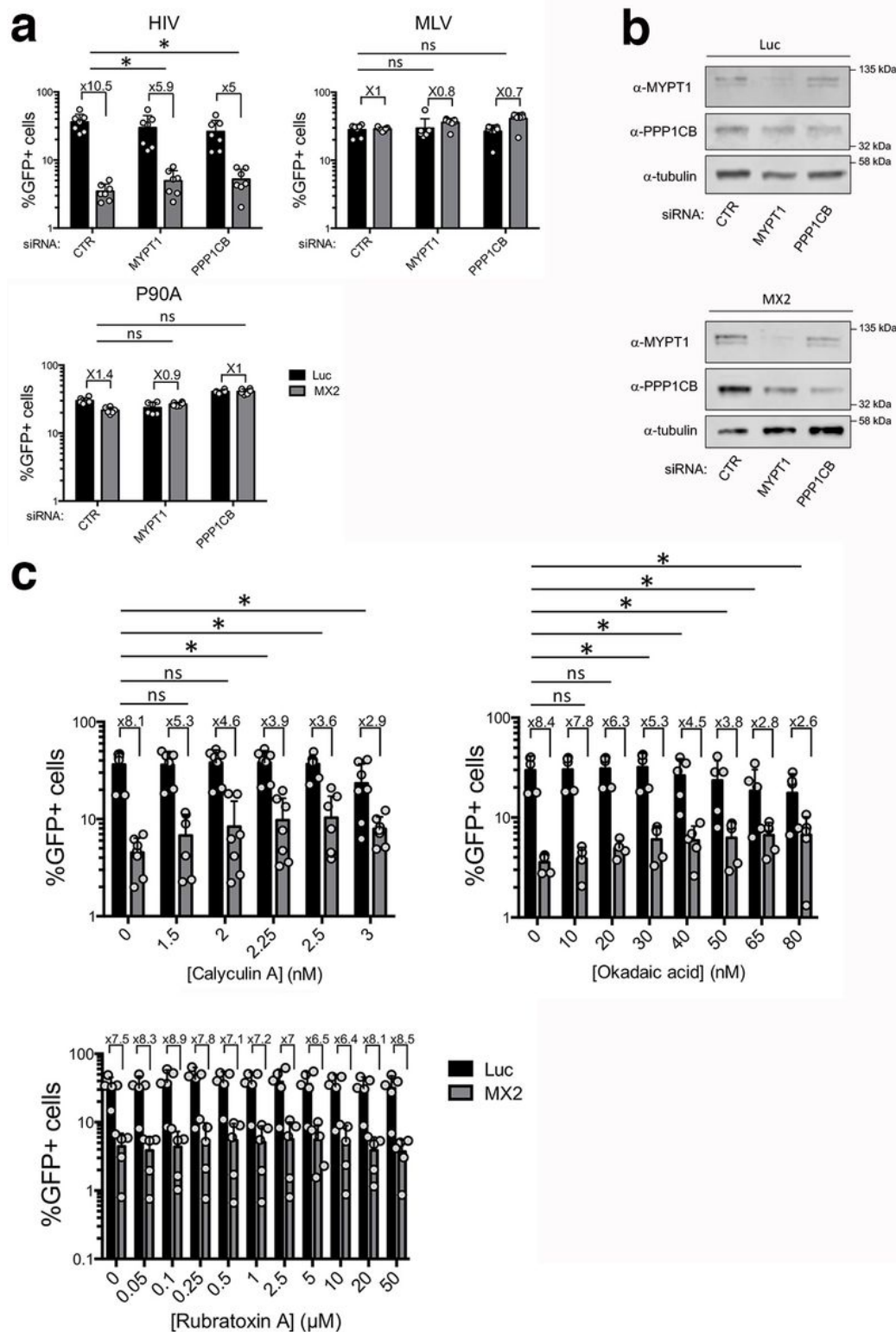


Figure 2

cytometry (n = at least 6, mean ± standard deviation (SD) *p value <0.05; two-tailed unpaired t-test). b, Immunoblot analysis of MYPT1 and PPP1CB depletion in U87-MG CD4+ CXCR4+ cells from panel A. Tubulin is included as a loading control. c, U87-MG CD4+ CXCR4+ cells expressing MX2 or Luc were treated with increasing concentrations of calyculin A, okadaic acid or rubratoxin A (or DMSO as a control) 6 h before challenge with HIV-1/GFP. Inhibitors were removed 24 h after addition and the percentage of infected cells enumerated at 48 h by flow cytometry (n = at least 4, mean ± SD, *p value <0.05, (ns) non-significant; two-tailed unpaired t-test).

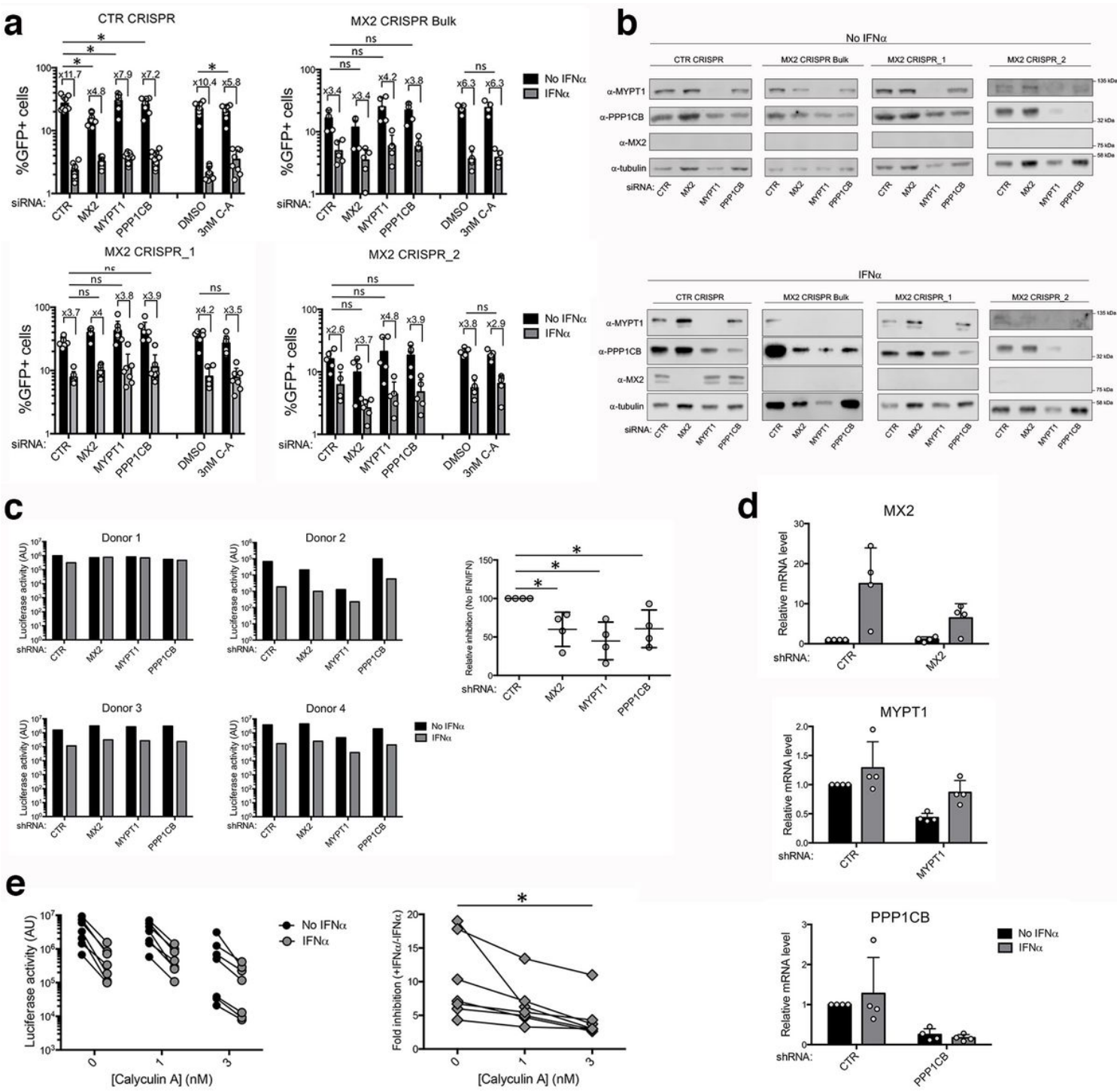


Figure 3

Lack of functional MLCP diminishes MX2-mediated inhibition of HIV-1 infection during the IFN response a, U87-MG CD4⁺ CXCR4⁺ cells transduced with a CRISPR-Cas9 control guide RNA, as well as a bulk population and two clonal cell lines where MX2 alleles had been disrupted by CRISPR-Cas9 genome editing, were either transfected twice with a control siRNA (CTR), or siRNAs targeting MX2, MYPT1 or PPP1CB, and treated or not with 500 U/ml IFN α for 24 h. Alternatively, cells were treated with 3 nM calyculin A (or DMSO) 6 h before infection and medium exchange 18 h later. Cells were challenged with HIV-1/GFP and infection enumerated at 48 h by flow cytometry (n = at least 5, mean \pm SD, *p value <0.05; two-tailed unpaired t test). b, Immunoblot analysis of MX2, MYPT1, PPP1CB and tubulin (loading control) in CTR CRISPR, MX2 CRISPR Bulk, MX2 CRISPR_1 and MX2 CRISPR_2 cells in the presence or absence of IFN α , and transfected with siRNAs (from panel A). c, Primary CD4⁺ T cells were isolated from 4 independent donors, transduced with shRNAs targeting MX2, MYPT1, PPP1CB or a scrambled sequence shRNA (CTR) and treated or not with 2,000 U/ml IFN α . At 24 h, cells were challenged with NL4.3/Nef-IRES-Renilla and luciferase activity determined 48 h later. Raw infectivity data are shown for each donor on the left (mean values from 3 technical replicates), and the fold inhibition of infection (no IFN/IFN) normalized to the CTR shRNA (assigned an arbitrary value of 100), on the right (*p-value <0.05; two-tailed paired t-test). d, Efficiency of MX2, MYPT1 or PPP1CB depletion in primary CD4⁺ T cells after shRNA transduction was quantitated by qPCR in the presence or absence of IFN α , normalizing to GAPDH. Data shown represent the 4 donors used in panel C. e, Primary CD4⁺ T cells isolated from 7 independent donors and treated or not with 2,000 U/ml of IFN α were incubated in the presence of DMSO or two concentrations of calyculin A (1 nM or 3 nM). After 6 h, cells were challenged with NL4.3/Nef-IRES-Renilla, the medium replaced 18 h later, and luciferase activity determined 48 h after infection. Raw infectivity data from all 7 donors are shown on the left and the fold inhibition of infection (no IFN/IFN), on the right (*p value <0.05; two-tailed paired t-test).

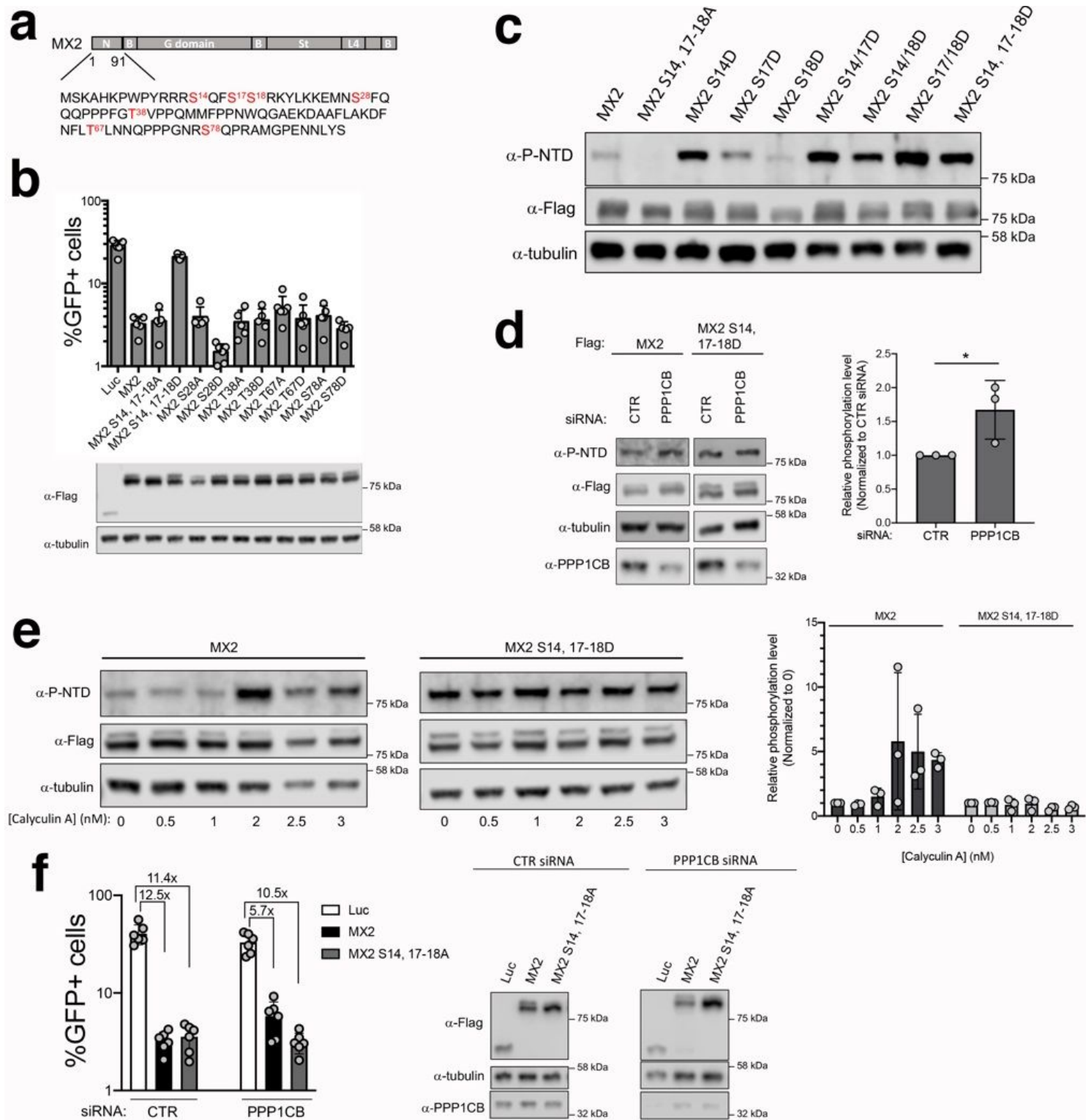


Figure 4

MX2 anti-viral activity is antagonized by phosphorylation a, MX2 domain organization showing the sequence of the N-terminal domain, and indicating residues found to be phosphorylated (in red). b, U87-MG CD4⁺ CXCR4⁺ cells were transduced with pEasiLV expressing Flag-tagged wild type or mutant MX2, or the Luc control. After induction with 0.5 μ g/ml of doxycycline for 48 h, cells were challenged with HIV-1/GFP and infectivity measured 48 h later (n = 5, mean \pm SD). The anti-Flag immunoblot shows MX2

expression levels, with tubulin as the loading control. c, Specificity of the anti-phosphorylated S14, 17-18 NTD antibody (anti-P-NTD) was defined using lysates from U87-MG CD4⁺ CXCR4⁺ cells expressing wild type or mutated MX2 proteins. Total protein expression (anti-Flag) is shown with tubulin serving as a loading control. d, MX2 or MX2 S14, 17-18D expressing U87-MG CD4⁺ CXCR4⁺ cells were doubly transfected with a siRNA targeting PPP1CB or a siRNA CTR. 48 h after the first transfection cells were lysed and the levels of MX2 phosphorylated at the S14-S17-S18 motif 861 (anti-P-NTD), total MX2 (anti-Flag) or PPP1CB determined by immunoblot. Tubulin was used as a loading control. Quantification of the level of phosphorylation, relative to the MX2 long isoform, and normalized to the CTR siRNA, is shown on the right (n = 3, mean \pm SD, *p value <0.05; two tailed unpaired t-test). e, DMSO (0) or increasing concentrations of calyculin A were used to inhibit MLCP in U87-MG CD4⁺ CXCR4⁺ cells expressing MX2 or MX2 S14, 17-18D. 6 h after treatment, cells were lysed and the levels of MX2 (anti-Flag), MX2 phosphorylated at the S14-S17-S18 motif (anti-P-NTD) or PPP1CB determined by immunoblot. Tubulin was used as a loading control. Quantification of the level of phosphorylation, relative to the MX2 long isoform, and normalized to the DMSO control condition, is shown on the right (n = 3, mean \pm SD, *p value <0.05; two-tailed unpaired t-test). f, U87-MG CD4⁺ CXCR4⁺ cells expressing Luc, MX2 or MX2 S14, 17-18A were transfected with a CTR siRNA or a siRNA targeting PPP1CB before being challenged with HIV-1/GFP and infectivity measured 48 h later by flow cytometry (n = 6, mean \pm SD). The fold inhibition by MX2 species, relative to Luc, is also shown. Fold inhibition for MX2 is significantly lower in PPP1CB siRNA treated cells compared to CTR siRNA treated cells (12.5x vs 5.7x; p value <0.05; two-tailed unpaired t-test), but not for MX2 S14, 17-18A (11.4x vs 10.5x). Protein expression was confirmed by immunoblot (right panel).

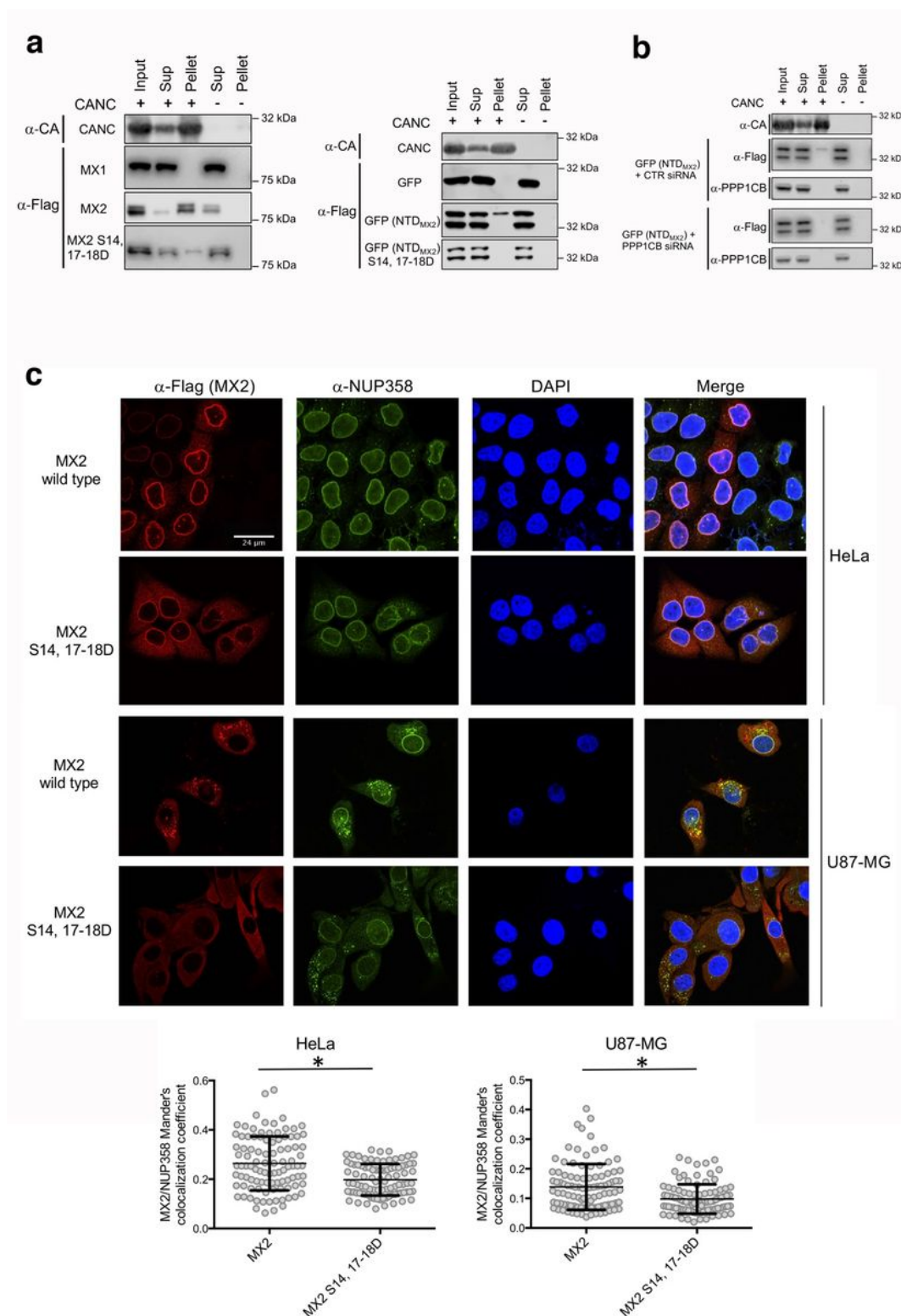


Figure 5

Phosphorylation of residues 14, 17 and 18 inhibits the 883 interaction of MX2 with the HIV-1 capsid and modulates its accumulation at the nuclear envelope a, 293T cells were transfected with pCAGGs vectors expressing Flag-tagged MX1, MX2, mutant MX2 S14, 17-18D, GFP, GFP (NTDMX2) or GFP (NTDMX2) S14, 17-18D. Cell lysates were incubated in the presence or absence of Capsid-Nucleocapsid (CANC) assemblies and subjected to centrifugation through a sucrose cushion. Supernatant (Sup) and Pellet

fractions, together with the Input sample, were analyzed by immunoblot using an anti-Flag antibody. A representative immunoblot for CANC (anti-CA) is shown. All experiments were done at least 4 times. b, 293T cells expressing GFP (NTDMX2) were transfected twice with a CTR siRNA or siRNA targeting PPP1CB, lysed and incubated with CANC assemblies. The resulting mixture was centrifuged through a sucrose cushion and resulting Sup and Pellet fractions, together with an Input sample, were analyzed by immunoblot using an anti-Flag antibody. A representative immunoblot for CANC (anti-CA) is shown. The efficiency of PPP1CB depletion was confirmed by immunoblot using an anti-PPP1CB antibody. All experiments were done at least 3 times. c, HeLa and U87-MG CD4⁺ CXCR4⁺ cells stably expressing wild type or S14, 17-18D mutant MX2 bearing a C-terminal Flag-tag were seeded onto glass coverslips. Localization of MX2, and endogenous NUP358 (a marker for the nuclear envelope) were determined by fluorescence confocal microscopy using anti-Flag and anti-NUP358 antibodies, respectively. DAPI was used to stain the nuclei. Below, colocalization of MX2 and NUP358 was quantified using Mander's coefficient for an average of 97 cells per condition, randomly selected (*p-value <0.05; two-tailed unpaired t-test)

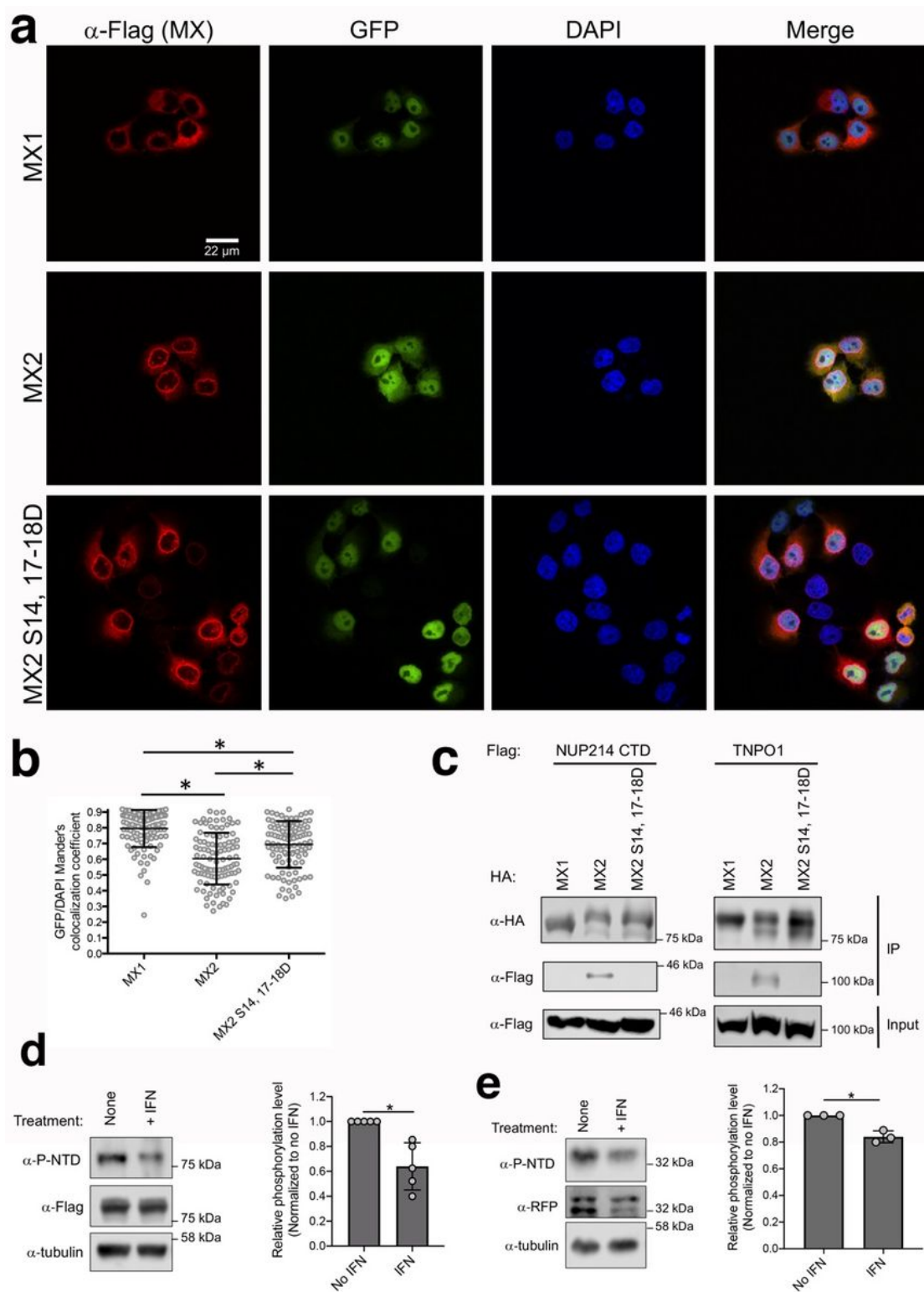


Figure 6

Phosphorylation of MX2 regulates interference with the nuclear import of cellular cargo a, HeLa cells stably expressing the HNRNP K (KNS)-GFP-LacZ chimera were transduced with puromycinR vectors expressing Flag-tagged MX1, MX2 or MX2 S14, 17-18D and selected for 48 h with puromycin before seeding on glass coverslips. MX proteins were detected using an anti-Flag antibody and the nuclei were stained with DAPI. b, Nuclear localization of KNS-GFP-LacZ was determined 914 for single cells by

quantifying colocalization with DAPI using Mander's coefficient for an average of 104 randomly selected cells (*p-value <0.05; two-tailed unpaired t-test). c, 293T cells were co-transfected with vectors expressing HA-tagged MX1, MX2 or S14, 17- 18D MX2 and Flag-tagged TNPO1 or a C-terminal fragment of NUP214. Cells were lysed and HA-tagged proteins immunoprecipitated and analyzed (together with input samples) by immunoblot using anti-Flag and anti-HA antibodies. All experiments were performed at least 3 times. d, U87-MG CD4+ CXCR4+ cells stably expressing Flag-tagged MX2 were treated or not with 1000 U/ml IFNa for 24 h before lysis and immunoblot analysis with anti-P-NTD or anti-Flag antibodies. Tubulin was used as a loading control. The level of MX2 phosphorylated at the S14-S17-S18 motif, relative to the MX2 long isoform, and normalized to the untreated condition was determined (n =5, mean \pm SD, *p-value <0.05; two-tailed unpaired t-test). e, RFP bearing the NTD of MX2 (RFP(NTDMX2)) was expressed in U87-MG CD4+ CXCR4+ cells. Cells were incubated or not with 1000 U/ml IFNa for 24 h, lysed and the level of phosphorylation at the S14-S17-S18 motif, relative to the RFP (NTDMX2) long isoform and normalized to the untreated condition, determined as in panel d (n =3, mean \pm SD, *p-value <0.05; two-tailed unpaired t-test).